



FRAS 1.1.3; Weld Residual Stresses

Simulated Behaviour of Welding Residual Stresses in NPP Primary Circuit Components Subject to Cyclic Loading

Author(s): Otso Cronvall

Confidentiality: Public




Report's title Simulated Behaviour of Welding Residual Stresses in NPP Primary Circuit Components Subject to Cyclic Loading	
Customer, contact person, address State Nuclear Waste Management Fund (VYR), BeräkningsGrupp (BG, members of which are TVO Oyj, Oskarshamn Ab, Ringhals Ab, Forsmark Ab) and VTT	Order reference(s) 5280-08; TVO, 4090234; Oskarshamn, 594100-003; Ringhals, 4500175143; Forsmark
Project name FRAS 1.1.3; Weld Residual Stresses	Project number/Short name 32418/FRAS 09
Author(s) Otso Cronvall	Pages 53 / 0
Keywords WRS, RS, NPP, piping component, weld, FEM	Report identification code VTT-R-02199-10
<p>Summary</p> <p>This study concerns the welding process induced residual stresses in Nuclear Power Plant (NPP) reactor circuit component welds, and their modelling for structural integrity analyses. The present study continues the work of the previous parts of the project. Here the emphasis is on numerical simulations of weld residual stresses (WRSs) and on how they alter/relax due to experienced repetitive mechanical loads. The same FEM model was used as in 2008 works, i.e. that consisting of a safe-end connecting to a nozzle and pipe. The scope of the analyses was extended so that here it was examined how the WRS distributions in the safe-end/pipe joint weld region behave under constant cyclic loading. Several load cycle sequences with different load amplitudes covering loading conditions ranging from moderate to relatively severe were used.</p> <p>Here as a starting point the initial WRSs were assumed according to the SINTAP procedure, as the WRS distributions it gives for welds connecting components of austenitic stainless steel were the least over conservative within the considered scope of commonly used WRS assumption procedures, see the other project report [1]. And unlike most of these commonly used procedures, SINTAP also gave in this case a self-balancing WRS distribution in perpendicular to weld direction, which is realistic.</p> <p>The Oak Ridge National Laboratory (ORNL) has created a material model to describe the behaviour of austenitic stainless steels of types 304 and 316. This model was used in the performed FEM analyses for the weld, safe-end and pipe materials, respectively. In this model the constitutive theory is uncoupled into a rate independent plasticity response and a rate dependent creep response, each of which is governed by a separate constitutive law. The plasticity theory uses a von Mises yield surface that can expand isotropically and translate kinematically in stress space.</p> <p>In the following is a brief description concerning the WRS simulation results:</p> <ul style="list-style-type: none"> • For all performed analyses, the load cycle sequences with larger stress load range decreased maximum WRS values more than those with smaller stress load range. • For load cycle sequences with stress ratio of 0; in the weld centre line the maximum tensional WRS values at inner surface decreased approximately from 28 to 60 %, depending on the case in question, whereas for maximum compression WRS values at outer surface this decrease was negligible. • For load cycle sequences with stress ratio of -1; in the weld centre line the maximum tensional WRS values at inner surface decreased approximately from 22 to 48 %, depending on the case in question, whereas for maximum compression WRS values at 	

outer surface this decrease was approximately from 9 to 54 %, respectively.

- Concerning the relaxation of the WRSs due to first load cycle as compared to that caused by the subsequent load cycles, it varied case specifically approximately from 50 to 80 % of the total WRS decrease.
- For all performed analyses in the weld centre line; within the wall the maximum WRS values both in tension and compression increased to some extent.
- For all performed analyses in the offset line which is located approximately 2.5 mm to the base material side from the weld edge; the maximum WRS values both in tension and compression decreased tens of percents both at inner & outer surface and slightly less so within wall.

Based on the conduct and outcome of the numerical FEM based simulations performed in this study it is concluded that this approach is feasible for modelling time dependently both the NPP components including the associated material properties, loads and boundary conditions, as well as the locally confined WRS fields and how they gradually alter/relax due to experienced repetitive mechanical load cycles.

The presented approach to assess numerically with FEM the relaxation of the WRSs could be well extended to other components having other materials and geometries without the needed computational work becoming too resource demanding.

Confidentiality	Public	
Espoo 26.4.2010		
Signatures	Signatures	Signatures
		
Written by Otso Cronvall Research Scientist	Reviewed by Juha Kuutti Research Scientist	Accepted by Eila Lehmus Technology Manager
VTT's contact address P.O. Box 1000, 02044 VTT		
Distribution (customer and VTT) SAFIR2010 Reference Group 6 (Structural Safety of Reactor Circuit); SAFIR2010 FRAS Ad-Hoc Group; BeräkningsGrupp (2+2+2+2); VTT Archive (2)		
<i>The use of the name of the VTT Technical Research Centre of Finland (VTT) in advertising or publication in part of this report is only permissible with written authorisation from the VTT Technical Research Centre of Finland.</i>		

Foreword

This report has been prepared under the research project FRAS 1.1.3; Weld Residual Stresses, which concerns welding process induced residual stress distributions in Nuclear Power Plant (NPP) reactor circuit component welds. The project is a part of SAFIR2010, which is a national nuclear energy research program. FRAS 1.1.3 project work in 2009 was funded by the State Nuclear Waste Management Fund (VYR), the BeräkningsGrupp (BG), and the Technical Research Centre of Finland (VTT). The work was carried out at VTT. The author of the report expresses his gratitude to Mr Paul Smeekes from Teollisuuden Voima Oyj (TVO) for valuable co-operation. The support from BG is also gratefully acknowledged.

Espoo 26.4.2010

Author

Contents

Foreword	3
List of symbols and abbreviations.....	5
1 Introduction.....	7
2 On the characteristics of WRSs.....	8
3 Numerical simulation of WRSs and their relaxation.....	10
3.1 Examined weld, initial WRSs, considered loads and other relevant input data	10
3.1.1 Geometry	10
3.1.2 Material properties	11
3.1.3 Loads	13
3.2 ORNL material model	15
3.3 Numerical heat transfer and stress/strain simulations.....	23
3.3.1 Boundary conditions	24
3.3.2 FEM model.....	25
3.4 WRS simulation results.....	27
4 Summary and suggestions for further research.....	48
5 Conclusions.....	51
References	52

List of symbols and abbreviations

Latin symbols

c	Specific heat
C	Constant related to the slope of the elastic-plastic line in initial loading stress-strain curve
E	Elastic modulus
E_p	Slope of the elastic-plastic line in initial loading stress-strain curve
I	Relative inelastic strain
L, N, M, G	Scalar functions denoting hardening characteristics of the material
p	Pressure
p_{\max}	Maximum pressure value
p_{\min}	Minimum pressure value
R	Stress ratio
S_{22}	Transverse to weld stress component
S_m	Design stress
S_u	Tensile strength
S_y	Yield strength
t	Time
t_{wall}	Component wall thickness
T	Temperature
W^C	Work due to creep strain
W^P	Work due to plastic strain

Greek symbols

α_{HT}	Heat transfer coefficient
α_{ij}	Components of total translation in deviatoric stress space of the loading surface during plastic or creep flow or both
α_T	Coefficient of thermal expansion
$\Delta \epsilon$	Strain range in cyclic stress-strain tests
$\bar{\epsilon}$	Effective strain
ϵ_{ij}	Total strain components, elastic-plastic strain tensor
ϵ_{ij}^C	Creep strain components
$\dot{\epsilon}_{ij}^C$	Creep strain rate components
ϵ_{ij}^E	Elastic strain components
ϵ_{ij}^P	Plastic strain components
ϵ_{ij}^T	Thermal strain components
$\bar{\epsilon}_{eq}^P$	Equivalent plastic strain according to Abaqus FEM code documentation
$\bar{\epsilon}_{0,eq}^P$	Initial equivalent plastic strain according to Abaqus FEM code documentation
$\dot{\bar{\epsilon}}^P$	Equivalent plastic strain rate according to Abaqus FEM code documentation
ϵ_{\max}	Maximum strain
ϵ_{\min}	Minimum strain

$d\varepsilon_{ij}^P$	Increments of plastic strain components
ϕ	Outer diameter
κ	Scalar characterising the size of the yield surface
κ_1	Tenth cycle value for the scalar characterising the size of the yield surface
λ	Thermal conductivity
ν	Poisson's coefficient
ρ	Density
σ_{ij}	Stress components
σ'_{ij}	Deviatoric stress components
σ_{\max}	Load cycle specific maximum stress value
σ_{\min}	Load cycle specific minimum stress value
σ_y	Yield stress, yield strength

Abbreviations

API	American Petroleum Institute
BG	BeräkningsGrupp
BWR	Boiling water reactor
FEM	Finite element method
LC	Load cycle
LCS	Load cycle sequence
MIG	Metal inert gas welding
NPP	Nuclear power plant
ORNL	Oak Ridge National Laboratory
PWHT	Post weld heat treatment
PWR	Pressurised water reactor
RPV	Reactor pressure vessel
SAW	Submerged arc welding
SCC	Stress corrosion cracking
SINTAP	Structural Integrity Assessment Procedures for European Industry
SMAW	Shielded metal arc welding
SO	Start of operation
SS	Stainless steel
TIG	Tungsten inert gas welding
TVO	Teollisuuden Voima Oyj
USNRC	U.S. Nuclear Regulatory Commission
VSR	Vibratory stress relief
VTT	Technical Research Centre of Finland
VYR	State Nuclear Waste Management Fund (Valtion Ydinjätehuoltorahasto)
WCL	Weld centre line
WOL	Weld offset line
WRS	Weld residual stress

1 Introduction

This report presents the performed numerical simulations concerning the behaviour of welding residual stresses (WRSs) in NPP primary circuit components subject to cyclic loading, carried out during 2009, and partly during 2010 as well. These simulation results have also been presented more briefly in the main research report concerning the project works of 2009, see ref. [1], which also covers a number of other aspects and issues concerning WRSs, including a literature study on WRS relaxation assessment procedures. In that report the scope concerning WRS simulations was mainly to develop analytical WRS relaxation assessment expressions based on the simulation results. Whereas this report is solely focused on these WRS simulations, and thus they are presented here with larger scope and in more detail. Which means that here are mainly presented such WRS simulation results that are not covered in the ref. [1].

This study represents the results concerning the third year, i.e. 2009, of a research project spanning four years, i.e. 2007 – 2010. A literature study concerning various commonly used WRS definition procedures was carried out in the first project year in 2007, see ref. [1]. In that study seven different WRS definition procedures were presented, reviewed and compared against each other for a representative set of relatively simple application examples concerning NPP reactor circuit piping welds. During the second project year 2008 it was studied with numerical simulations how the WRSs alter over the years in plant operation in primary circuit component welds, due to various typical/anticipated transient load cases, see ref. [3]. The target of application was from a Finnish Boiling Water Reactor (BWR) unit. With such stress results, it was then examined what is their impact to the corresponding simulated crack growth rates. In the latter analyses a fracture mechanics based analysis tool was used.

The present study continues the work of the previous parts of the project. As mentioned above, here the focus is on the performed numerical WRS simulations concerning NPP primary circuit component welds. These simulations were carried out with the same finite element method (FEM) model as was used in 2008, i.e. that consisting of a safe-end connecting to a nozzle and pipe. The scope of the analyses was extended so that here it was examined how the WRS distributions in the safe-end/pipe joint weld region behave under constant cyclic loading. Several load cycle sequences with different load amplitudes covering loading conditions ranging from moderate to relatively severe were considered.

After this introductory chapter, the characteristics of WRSs in metallic components are briefly described in Chapter 2. The main focus is on NPP components.

The above mentioned FEM simulations of WRSs in the safe-end/pipe joint weld region are described in Chapter 3. This includes describing the needed analysis input data and the FEM model, and presenting the analysis results. The analyses cover eight loading histories, each including a constant amplitude load cycle sequence, and together spanning a representative range of loading conditions.

Chapter 4 presents summary and suggestions for further research.

Finally, conclusions concerning the whole study are presented in Chapter 5.

2 On the characteristics of WRSs

Assessment of the structural integrity of critical components and structures in NPPs is of remarkable importance for safe operation. When assessing the structural integrity of a component, both the loading and the load-carrying capacity are determined. The WRSs are included in the analysis on either the loading or capacity side, depending on the design strategy.

Since WRSs with various magnitudes and distributions are present in virtually all structurally engineered components, there is a demand for accurate assessment of the WRS distributions, especially in critical components. The residual stress distributions present in a structure are the result of the manufacturing history and the elastic-plastic properties of the structure. The former referring to the mechanical and thermal processes executed during the whole production sequence and the latter to the elastic-plastic behaviour of the structure. Because the elastic-plastic properties influence the severity and distribution of the WRSs, it follows that a structure comprised of several materials will experience the development of the WRSs in a completely different way than one made of a single material.

Depending on the importance of the WRSs, different approaches have been introduced for the assessment of the structural integrity. In structures where the effect of the WRSs on the performance is limited or small, the assessment of the WRSs is of less importance. On the other hand, in the structures where their integrity is of remarkable importance for their reliability, such as NPP primary circuit components, a thorough and accurate assessment of the WRS state is of primary concern. NPPs are typically concerned with manufacturing and managing components which are strongly regulated by national and/or international technical guidelines, standards and design codes to ensure reliable operation.

WRSs are defined as static mechanical stresses that are present in a thermodynamically (and mechanically) closed system of equilibrium. In a more general way, WRSs are mechanical stresses that exist in a component without any external applied mechanical or thermal loads. A direct consequence of the definition is that all internal forces and moments resulting from the WRSs of a system are in mechanical equilibrium. The size of the considered system determines the type of the WRSs that are assessable.

Another consequence of the above mentioned definition is that the internal stresses induced by thermal transients are outside the scope of the WRSs, as they do not represent closed systems. Such load transients are typical for uneven cooling during heat treatments and thermal in-service loads. However, the thermal transients can induce WRSs, when the yield strength is exceeded locally and plastic flow occurs.

The mechanical properties that govern the formation of WRSs are primarily the modulus of elasticity and the strain hardening coefficient. In the case of a work hardening material the WRSs are completely different than for a work softening material. Thus, a mismatch in strain hardening capabilities in adjoining materials, with otherwise similar elastic properties, induces local plastic deformation in the weaker material.

One notable issue concerning these locally confined WRSs in NPP components is that their peak values can be relatively high. For instance, concerning the structural integrity analyses of NPP components, in the commonly applied fitness-for-service procedures it is typically

assumed that the maximum tensile initial WRS values are of the magnitude of yield strength in and near the component inner surface. Moreover, it is usually further assumed that if the weld has not experienced any improving treatment, the WRSs remain in the initial as-welded state values. This hardly seems appropriate for components in such NPPs that have been in operation for decades. How the operational conditions and anticipated/experienced plant load transients may gradually relax the WRSs in NPP components during several years of operation has for the time being remained as a surprisingly little examined issue.

Manufacturing of welded structures in NPPs is carried out with such traditional methods concerning which there is considerable welding experience. The methods are Shielded metal arc welding (SMAW), Tungsten inert gas welding (TIG) and Submerged arc welding (SAW). However, Metal inert gas welding (MIG) is generally not used due to a higher risk for lack of fusion. Manufacturing of clad structures is a time consuming process, and therefore it is mostly done with SAW. Other methods have also been used, though less frequently. Butt welding of pipes, on the other hand, is made with TIG.

Regardless of the welding method used, the material properties of the welds and the structural materials affect the formation and distribution of WRSs. The resulting WRS state in a welded component is determined by welding related parameters and geometrical constraints. The former refers to the local shrinkage, quench and phase transformations resulting from the localised thermal cycle. The latter is dealt with through the unbalance in material properties of dissimilar metal welds, and the constraining effect of the surrounding structure.

The components of primary interest in NPPs often have a bi-metallic or dissimilar metal structure, where the mechanical properties of the joined materials are different, and thus add to the formation of the WRSs. However, in most cases NPP primary circuit welds are similar, i.e. same materials are joined in a weld.

In the assessment of the WRS distributions in NPP components, the possible relaxation of the former by post processing or during service operation is necessary to be taken into account.

It is a generally known fact that there are three primary sources for WRS redistribution or relaxation. These are as follows:

- Irradiation effects; Irradiation is not used in practise to relax the WRSs in NPP components. Besides NPP reactor pressure vessel (RPV) and its internals, the effect of irradiation to other metallic NPP components is negligible [9].
- Thermal effects; The operational temperatures of Boiling water reactor (BWR) and Pressurised water reactor (PWR) units are too low for creep to relax the WRSs. Thermal treatments used in relaxing the WRSs include post weld heat treatment (PWHT).
- Mechanical load effects; WRS relaxation is associated with static or cyclic mechanical load applied to the component to cause local plastic yielding, which redistributes/relaxes the residual stresses. Treatments used in relaxing the WRSs include shot-peening (which is a surface treatment) and vibratory stress relief (VSR).

3 Numerical simulation of WRSs and their relaxation

The NPP primary circuit components analysed here are a safe-end connecting to a nozzle and pipe, resembling those that connect the feed water system to the RPV in BWR units. In particular, it is examined how to simulate with FEM the WRS distributions and their behaviour for of a number of different constant amplitude load cycle sequences in the safe-end/pipe weld joint. The as-welded state WRS distribution for this weld is assumed according to SINTAP procedure [5, 6]. The analysis tool selected for numerical simulations is Abaqus [12, 13], which is an advanced general purpose FEM analysis code, allowing time dependent 2D and 3D elastic-plastic analyses.

Here the needed analysis input data including geometry and material properties are presented first. The applied time dependent load cases, being load cycle sequences with different case specifically constant load amplitudes, are described next. Then the material model used here for components of austenitic stainless steel (SS) is described in more detail. The prepared FEM model is presented next, together with the associated boundary conditions. This follows with a description of the performed heat transfer and stress/strain FEM simulations. Finally, the WRS simulation results are presented.

3.1 Examined weld, initial WRSs, considered loads and other relevant input data

3.1.1 Geometry

The general geometry of the analysed BWR primary circuit components is presented in the following Figures 3.1.1-1 and 3.1.1-2.

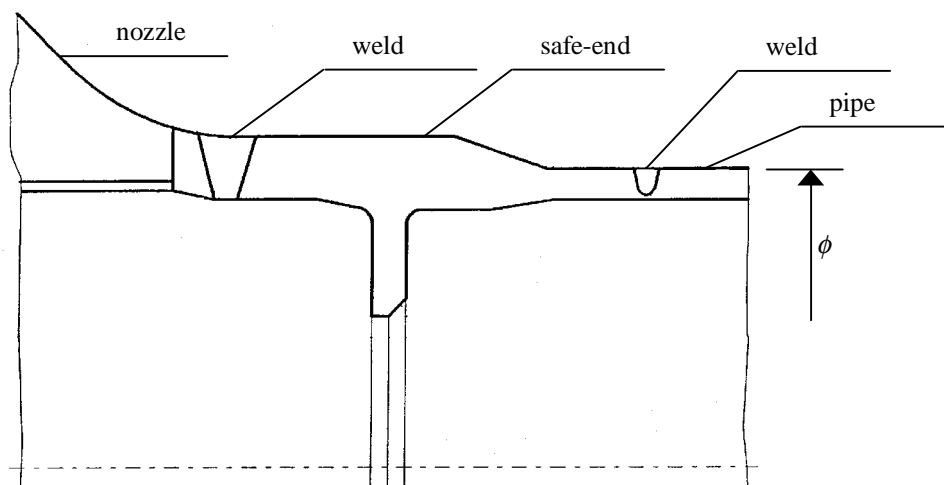


Figure 4.1.1-1. The overall geometry of the safe-end connecting to a nozzle and pipe, resembling those that connect the feed water system to the RPV in BWR units; horizontal section of the components at the level of their common symmetry axis. The outer diameter ϕ is of the scale of a few hundred mm.

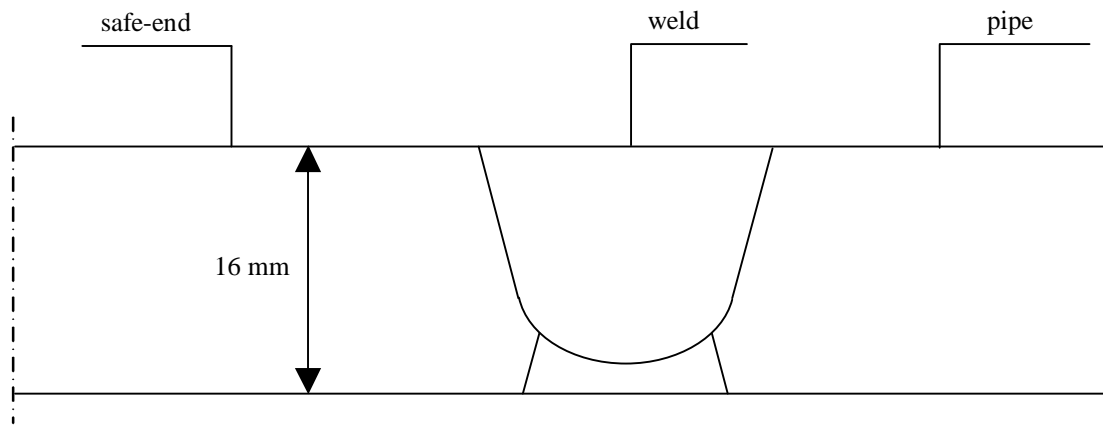


Figure 3.1.1-2. Geometry detail of the analysed safe-end/pipe joint weld, for its location see Figure 3.1.1-1.

3.1.2 Material properties

The material types of the components covered in the numerical simulations are listed in Table 3.1.2-1.

Table 3.1.2-1. Material regions of the analysed nozzle, safe-end and pipe, together with joining welds.

Component	Location	Material Type
Nozzle	Base material	Ferritic steel
Nozzle/safe-end weld	Beads & root	Austenitic weld material
Safe-end	Base material	Austenitic SS
Safe-end/pipe weld	Beads & root	Austenitic weld material
Pipe	Base material	Austenitic SS

The material properties of the austenitic SSs considered in the FEM analyses are presented in the following in Tables 3.1.2-2 to 3.1.2-6.

Table 3.1.2-2. Strength properties of the austenitic SS safe-end material and austenitic weld material, the values were taken from ref. [11].

Temperature T [°C]	Yield strength (*) S_y [MPa]	Design stress S_m [MPa]	Tensile strength S_u [MPa]
21	241	137	586
93	229	137	586
149	223	137	586
204	220	137	586
260	220	137	586
286	220	137	586
316	220	137	586

(*): 1.2 times these values were used as yield strength values corresponding to tenth load cycle, which is an extrapolated approximation based on material data presented for austenitic SS of type 304 in ref. [14].

Table 3.1.2-3. Strength properties of the austenitic SS pipe material, the values were taken from ref. [11].

Temperature T [°C]	Yield strength (*) S_y [MPa]	Design stress S_m [MPa]	Tensile strength S_u [MPa]
20	172	115	483
100	146	115	452
150	132	115	421
200	121	110	406
250	114	103	398
275	111		
300	108	97.7	393

(*): 1.2 times these values were used as yield strength values corresponding to tenth load cycle, which is an extrapolated approximation based on material data presented for austenitic SS of type 304 in ref. [14].

Table 3.1.2-4. Some mechanical properties of the austenitic SS safe-end material and austenitic weld material, the values were taken from ref. [11].

Temperature T [°C]	Elastic modulus E [GPa]	Thermal conductivity λ [W/m°C]	Specific heat c [J/kg°C]	Coefficient of thermal expansion $\alpha_T \cdot 10^{-06}$ [1/°C]
21	213.7	14.9	451	12.2
38		15.1	456	12.4
66		15.4	464	12.7
93	208.2	15.8	471	13.0
121		16.1	475	13.2
149	206.2	16.6	485	13.3
177		17.0	486	13.5
204	203.4	17.5	494	13.6
232		17.8	495	13.8
260	199.9	18.3	501	13.9
288		18.7	507	14.0
316	197.9	19.2	515	14.1

Table 3.1.2-5. Some mechanical properties of the austenitic SS pipe material, the values were taken from ref. [11].

Temperature T [°C]	Elastic modulus E [GPa]	Thermal conductivity λ [W/m°C]	Specific heat c [J/kg°C]	Coefficient of thermal expansion $\alpha_T \cdot 10^{-06}$ [1/°C]
21	195	14.9	484	15.2
38		15.1	486	15.4
66		15.6	496	15.6
93	190	16.1	506	15.8
121		16.6	516	16.0
149	186	17.0	520	16.2
177		17.5	529	16.4
204	183	18.0	535	16.5
232		18.3	539	16.7
260	178	18.9	544	16.9
288		19.2	548	17.0
316	174	19.6	551	17.2

Table 3.1.2-6. Values of density and Poisson's coefficient for the considered materials, which values were taken from ref. [11].

Material	Density ρ [kg/m ³]	Poisson's coefficient ν [-]
austenitic SS safe-end material	8430	0.3
austenitic SS pipe material	7850	0.3

3.1.3 Loads

The stresses and strains experienced by the analysed safe-end as well as connected nozzle and pipe are induced by various assumed load cases and types of loads. The WRSs as well as transient and stationary load cases considered in the heat transfer the stress/strain analyses are presented in the following. Also, the dead weights of the analysed components were considered, based on their dimensions and material densities.

WRSs

The stationary welding process induced residual stresses for the analysed safe-end/pipe joint weld are presented in the following. As mentioned earlier, SINTAP procedure [5, 6] is selected for assessing the as-welded state WRSs to be used in the FEM simulations in this study.

As for the yield strength of the considered austenitic SSs, the work hardening after the beginning of the plastic deformation must be taken into account as well. In this case, the yield strength σ_y is defined as the 1.0 % proof stress. To a first approximation: σ_y ($\sigma_y = 1.0$ %) $\approx 1.5 \cdot \sigma_y$ ($\sigma_y = 0.2$ %), as recommended in the SINTAP procedure documentation [5, 6]. The temperature is set to 286 °C for the most part of each calculation, corresponding to operational temperature in Finnish BWR NPP units. In this temperature the stress at 0.2 % strain of the considered austenitic weld material is 220 MPa. Here 1.5 times the stress at 0.2 % strain, i.e. 330 MPa, was taken to correspond to the stress at 1.0 % strain.

The as-welded state WRSs defined according to SINTAP procedure [5, 6] for the analysed safe-end/pipe joint weld in perpendicular to weld direction are presented in the following Table 3.1.3-1

Table 3.1.3-1. WRS input data for numerical simulations concerning the examined safe-end/pipe joint weld.

WRS definition procedure	SINTAP, see refs. [5, 6]
WRS direction	axial
WRS value in inner surface at 20/286 °C [MPa]	269/245
WRS value in outer surface at 20/286 °C [MPa]	-269/-245
Variation of WRS between inner/outer surface	linear

Cyclic loads

The main cyclic loading used in the analyses here, see Table 3.1.3-2, was applied in the form of even stress distribution over the pipe end cross-section surface, i.e. load sequence specifically it varies only as a function of time. The direction of the stress loading is axial, i.e. parallel to the common symmetry axis of the considered components. Also inner pressure was a cyclically altering load parameter here. Altogether eight different load cycle sequences (LCSs) were prepared. They all are constant amplitude load sequences with linear altering of the loading parameter values within the respective loading ranges. The rising and decreasing load cycle parts are separated with parts of static loading conditions having the same duration as the neighbouring altering parts. All prepared load cycles (LCs) end up to the same loading conditions as they start with. The prepared load cycle sequences cover a representative range of stress amplitudes from moderate up to relatively severe loading conditions.

The loading events considered in the heat transfer and the stress/strain simulations were applied as load histories. Also, the dead weights of the analysed components were considered, based on their dimensions and material densities. Each considered load history started with the loading of the WRSs, during which event no other mechanical loads were present and the overall temperature was kept at 20 C°. Following that, the pressure and temperature were elevated to the values corresponding to the operational conditions, those being for the considered BWR environment pressure of 70 bar and temperature of 286 °C, respectively. This was realised with a load event called here Start of operation (SO), resembling typical plant load transient Cold start-up. For all considered load histories these first two load events were exactly the same, with their durations being 3000 and 27000 s, in the respective order of their occurrence. Then followed the load history specific LCS, ending itself and at the same time the considered load history to steady state. Altogether eight load histories are covered, and correspondingly eight separate FEM analyses were performed. A diagram showing in principal the two types of prepared LCs is presented in Figure 3.1.3-1 in the following. For both types a set of five LCs are shown in this figure, corresponding to the performed FEM analyses where the covered LCSs were composed of step assemblies with ten of LC sets in each.

Table 3.1.3-2. Load cycle sequence (LCS) data for numerical simulations concerning the safe-end/pipe joint weld. The cyclic loads are: even stress distribution perpendicular to the weld and acting over the pipe end cross-section surface, and internal pressure. Here σ_{min} and σ_{max} denote minimum and maximum axial stress loads, whereas p_{min} and p_{max} denote minimum and maximum inner pressure loads, respectively, and LC means a single load cycle.

LCS No.	σ_{max} [MPa]	σ_{min} [MPa]	$R = \sigma_{min}/\sigma_{max}$	p_{max}/p_{min} [bar]	Temperature [°C]
1	150	0	0	70.0/1.0	286
2	100	0	0	70.0/1.0	286
3	50	0	0	70.0/1.0	286
4	25	0	0	70.0/1.0	286
5	150	-150	-1	70.0/1.0	286
6	100	-100	-1	70.0/1.0	286
7	50	-50	-1	70.0/1.0	286
8	25	-25	-1	70.0/1.0	286
LC Rising/Decreasing/Static Part Durations [s]					100/100/100
LC Duration [s]					400
No. of LCs in LCS					10 x 5

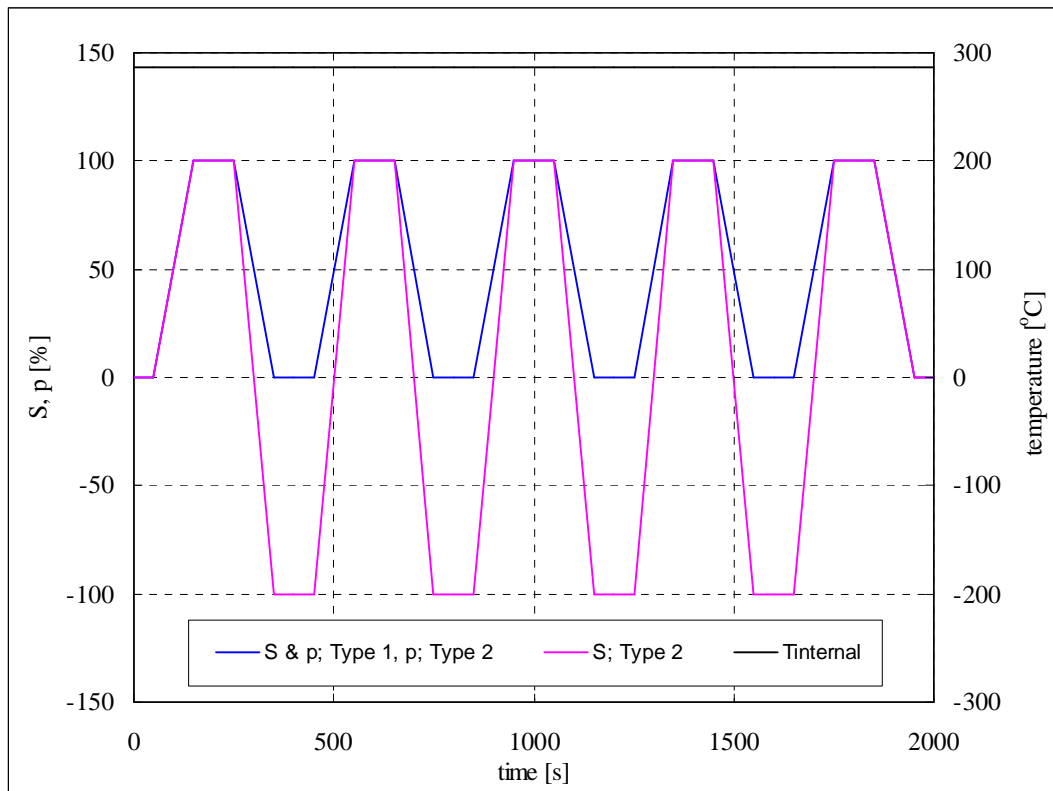


Figure 3.1.3-1. A diagram showing in principal the two types of prepared load cycles. Here S is axial stress at pipe end, p is internal pressure, Type 1 corresponds to LCSs from 1 to 4, and Type 2 corresponds to LCSs from 5 to 8, respectively. For S and p the shown values are percents of the respective LC specific maximum value, and when being on the negative side they correspond to compression. T_{internal} is internal temperature.

3.2 ORNL material model

The Oak Ridge National Laboratory (ORNL) has created a material model to describe the behaviour of austenitic SSs of types 304 and 316, see the Nuclear Standard NE F9-5T [14]. This model was used in the performed FEM analyses for the weld, safe-end and pipe materials, respectively. In this model the constitutive theory is uncoupled into a rate independent plasticity response and a rate dependent creep response, each of which is governed by a separate constitutive law. The plasticity theory uses a von Mises yield surface that can expand isotropically and translate kinematically in stress space.

The ORNL material model for austenitic SSs of types 304 and 316 according to [14] is described in more detail in the following. The scope is limited here to elastic-plastic analysis, i.e. the above mentioned plasticity response, as within the operational temperature range of NPPs the effect of creep is negligible as compared to the plasticity response, and in general as well.

The method of calculation is based on the assumption that the total strain at any instant of time consists of four parts: thermal, elastic, plastic, and creep. It is generally considered that time increment specifically elastic-plastic strains and creep strains are computed separately

and added together. The strains accumulated during the expected operating lifetime and loading history should be determined by summing the strains computed for each time increment as follows:

$$\varepsilon_{ij} = \varepsilon_{ij}^T + \varepsilon_{ij}^E + \int d\varepsilon_{ij}^P + \int \dot{\varepsilon}_{ij}^C dt \quad (3.2-1)$$

where time increment specifically ε_{ij} are total strain components, ε_{ij}^T are thermal strain components, ε_{ij}^E are elastic strain components, $d\varepsilon_{ij}^P$ are increments of plastic strain components, $\dot{\varepsilon}_{ij}^C$ are creep strain rate components, and dt are time increments.

Initial and subsequent yield condition hardening rules

The recommended yield condition specifying the initial yield surface and subsequent loading surfaces is given by:

$$f = (1/2) \cdot (\sigma'_{ij} - \alpha_{ij}) : (\sigma'_{ij} - \alpha_{ij}) = \kappa, \quad (3.2-2)$$

with evolution laws as:

$$d\kappa = L \cdot d\bar{\varepsilon}^C + N \cdot d\bar{\varepsilon}^P + M \cdot dt \text{ for isotropic hardening contribution,} \quad (3.2-3)$$

$$d\alpha_{ij} = G \cdot d\varepsilon_{ij}^P \text{ for kinematic hardening contribution,} \quad (3.2-4)$$

where: σ'_{ij} are deviatoric stress components, α_{ij} are components of total translation in deviatoric stress space of the yield surface centre point during plastic or creep flow or both, κ is scalar characterising the size of the yield surface, ε_{ij}^P , ε_{ij}^C are plastic and creep strain components, respectively, L , N , M , G are scalar functions denoting hardening characteristics of the material and are expressed in more detail further here, and T is temperature.

The presently outlined theory can be thought of as "nearly" linear kinematic hardening, i.e. the dependence of κ on inelastic strain is not strong and G in equation (3.2-4) is "almost" a constant. When κ is used as defined in equation (3.2-3), then the corresponding form for equation (3.2-4) is:

$$d\alpha_{ij} = C \cdot d\varepsilon_{ij}^P - \frac{N}{2 \cdot \kappa} d\bar{\varepsilon}^P \cdot S_{ij}, \quad (3.2-5)$$

where C is a material characterization parameter to be defined more specifically further here, $d\bar{\varepsilon}^P$ is effective plastic strain component, for calculation of effective strain components in general see equation (3.2-11), and:

$$S_{ij} = \sigma'_{ij} - \alpha_{ij} \quad (3.2-6)$$

Flow rule

The flow rule associated with the yield condition, i.e. equation (3.2-2), the specified hardening rules, i.e. equations (3.2-3) and (3.2-5), and the condition of normality is given by:

$$d\varepsilon_{ij}^P = S_{ij} \cdot d\Sigma / (2 \cdot C \cdot \kappa), \quad \text{if } f = \kappa \text{ and } d\Sigma > 0, \quad (3.2-7a)$$

and:

$$d\varepsilon_{ij}^P = 0, \quad \text{if } f \neq \kappa \text{ or } f = \kappa \text{ and } d\Sigma \leq 0, \quad (3.2-7b)$$

in which:

$$d\Sigma = S_{ij} : d\sigma_{ij} - M \cdot dT - L \cdot d\bar{\varepsilon}^C \quad (3.2-8)$$

and $d\sigma_{ij}$ are increments of stress components.

Bilinear representations of stress-strain curves

The basis here is the initial monotonic loading stress-strain curves. Correspondingly, the initial values of the three material properties, namely E , C and $\kappa = \kappa_0$, are determined from the bilinear representation of the initial loading stress-strain curve. Analyses beyond initial loadings are to accommodate the hardening influence of accumulated inelastic strain through the use of κ values that differ from κ_0 . These values of κ are determined from cyclic stress-strain loops. In most cases, the limiting value of κ corresponds to that for the tenth cycle of fixed strain range cycling and is denoted by κ_1 . Procedures for making the changes in κ are provided further here.

Bilinear representations of initial monotonic stress-strain curves are described in the following. For each temperature, the constants E , C and κ_0 to be used in a specific initial loading elastic-plastic analysis should be determined from bilinear representations of appropriate stress-strain curves for monotonic uniaxial tensile loading of virgin material. The procedures for evaluating the constants are given below and illustrated in Figure 3.2-1.

The following information is associated with the Figure 3.2-1:

- a) The elastic segment of the bilinear curve, represented by straight line OA whose slope is E , is determined by the initial response of the material.
- b) For a given maximum elastic-plastic strain, the elastic-plastic segment of the bilinear curve is determined by straight line BC connecting the stress point at the maximum strain ε_{\max} to the stress point at strain $\varepsilon_{\max}/2$.
- c) The yield point, σ_0 , is defined as the intersection of these two straight lines at A.
- d) The value of κ_0 is determined from the yield point σ_0 by the relation:

$$\kappa_0 = (1/3) \cdot \sigma_0^2 \quad (3.2-9)$$

e) The constant C is related to the slope E_p of the elastic-plastic line by the relation:

$$C = (2/3) \cdot (E \cdot E_p) / (E - E_p) \quad (3.2-10)$$

Correlations of data therefore should provide $E(T)$, $C(\epsilon_{\max}, T)$ and $\kappa_0(\epsilon_{\max}, T)$. The choice of the maximum strain to be used in selecting the appropriate bilinear representation must be left to the judgment and experience of the designer. Usually, the maximum strain chosen should correspond to the maximum elastic-plastic strain levels generally expected in the structure. In most realistic design situations, a maximum strain of not more than 0.2 or 0.3 % would be appropriate. This is an important point; maximum strain values much higher than this will result in unrealistically high initial yield points and unrealistically low plastic slopes. In multi-axial strain states, the maximum strain should be assessed on the basis of an effective strain value $\bar{\epsilon}$ at a point, defined by:

$$\bar{\epsilon} = (2 \cdot \epsilon_{ij} : \epsilon_{ij} / 3)^{0.5} \quad (3.2-11)$$

where ϵ_{ij} represents the elastic-plastic strain tensor.

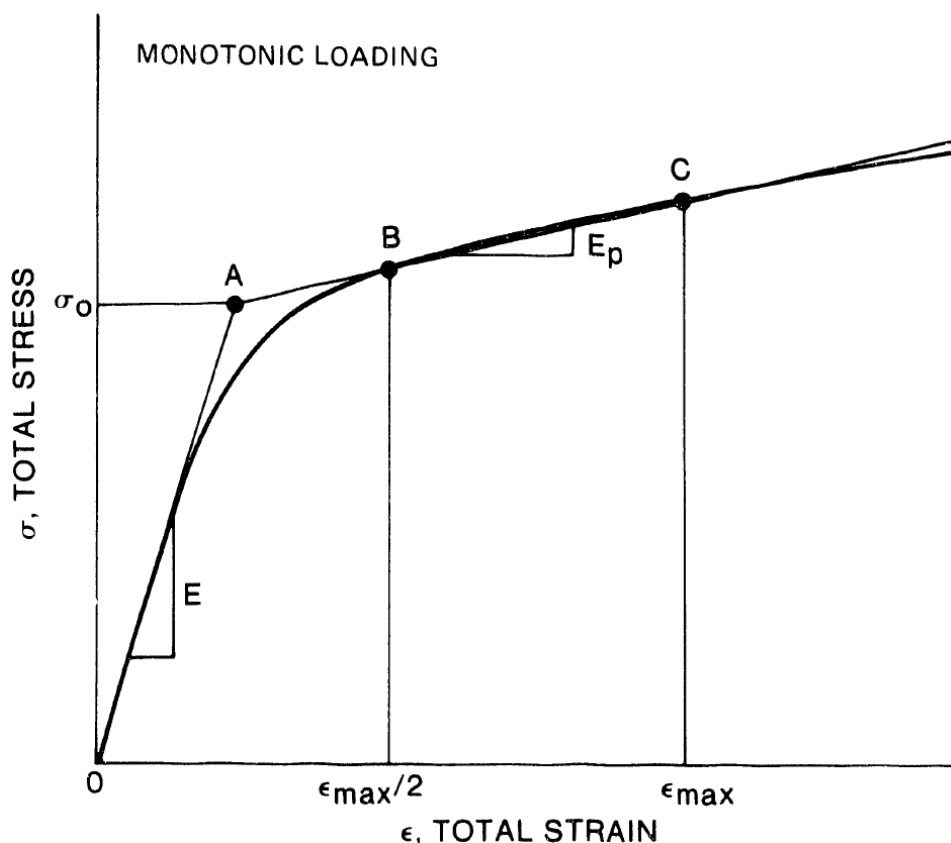


Figure 3.2-1. Bilinear representation of monotonic, initial loading stress-strain curve.

Bilinear representations of cyclic stress-strain curves are described in the following. Calculations for loadings beginning with the first reversed inelastic loading should generally be based on bilinear representations of cyclic stress-strain curves obtained from uniaxial tests of specimens cycled between fixed strain limits $\pm\epsilon_{\max}$. The procedure for determining the

bilinear representation of a given cyclic stress-strain curve is given below and illustrated in Figure 3.2-2.

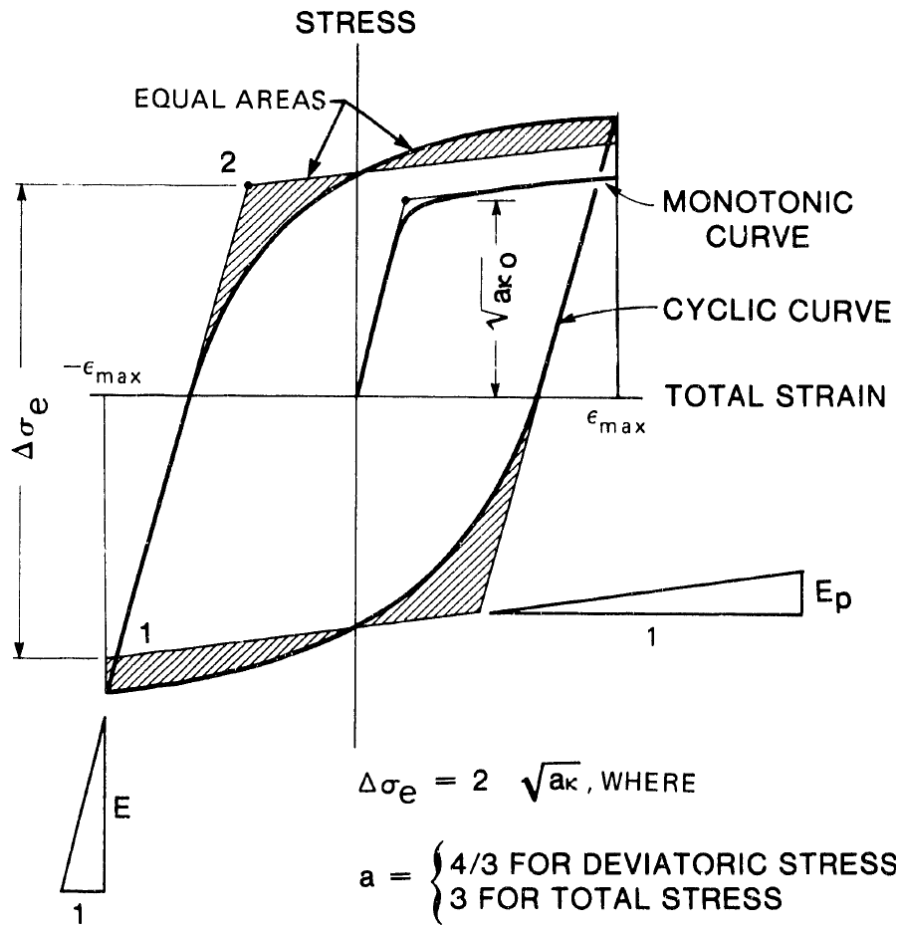


Figure 3.2-2. Bilinear representations of the initial and cyclic stress-strain curves.

The value of ϵ_{\max} used in this cyclic procedure should normally be the same as that used in the initial monotonic procedure described above. However, a smaller value of ϵ_{\max} may be used that corresponds to half the range of cyclic strain expected in the structure, rather than to the maximum strain expected. This smaller value of ϵ_{\max} may be used for evaluation of κ alone, or for evaluation of both C and κ .

The following information is associated with the Figure 3.2-2:

- a) For a given temperature and ϵ_{\max} the slope of the plastic portion of the bilinear representation of a cyclic stress-strain curve (and consequently the value of C) is equal to that of the bilinear representation of the initial monotonic stress-strain curve for the same temperature and ϵ_{\max} .
- b) The intersections of the elastic and elastic-plastic lines are located so that the areas above and below the actual curve are approximately equal. That is, the two shaded areas on the tensile (positive stress) portion of the cyclic curve shown in Figure 3.2-2 are equal, and the shaded areas on the compressive portion are equal.

c) The value κ is determined from the points of intersection of the elastic lines with the elastic-plastic lines as shown in Figure 3.2-2. The slope of the elastic line is E , and the slope of the elastic-plastic line is:

$$E_p = (3/2) \cdot (E \cdot C) / [E + (3/2) \cdot C] \quad (3.2-12)$$

d) The quantity κ is related to the elastic total stress range $\Delta\sigma_e$ of the equivalent bilinear cyclic curve by the relation:

$$\kappa = (1/12) \cdot \Delta\sigma_e^2 \quad (3.2-13)$$

Procedures for Selecting or Changing κ

The basic model recommended earlier for defining κ recognizes that the material in a structure can be hardened by prior loadings, and that the use of stress-strain data from virgin material can lead to predictions of larger plastic strains than will actually occur in some applications. However, the sole use of information obtained from material after hardening has occurred could give first loading predictions that are grossly in error. Therefore, when they are important, predictions of the first inelastic loadings should use the κ_0 value from initial monotonic loading tensile tests. The κ value is then changed during plastic loading. The changes should generally be made locally.

There are the following three permissible ways of selecting or changing κ :

- a) use a single hardened value throughout,
- b) make a step change to the hardened value, or
- c) change κ continuously until the hardened value is reached.

Method a) places an emphasis only on a representative modelling of long term cyclic response, while method c) includes an emphasis on a more accurate representation throughout the stages of loading. Method b) attempts to capture both the initial and hardened state in a single fashion.

Of methods b) and c) above for changing κ , the latter is more in keeping with observed material behaviour, and it avoids the computational difficulties and inconsistencies that sometimes accompany step changes. In all cases, changes in κ are limited to a maximum value, κ_{\max} . For most applications the limiting value is $\kappa_{\max} = \kappa_1$, the latter being the tenth cycle value, however, also other choices are possible.

Continuous Changes in κ

Continuous changes in κ are more consistent with data than the step change option. Nevertheless, as with the step change option, data indicate that hardening is limited to the final hardened value κ_{\max} . In general, $\kappa_{\max} \geq \kappa_1$, as discussed earlier. Existing data indicate that L and N of equation (3.2-3) defining continuous changes are both positive scalar functions of inelastic strain and temperature.

Utilisation of continuous changes obviously couples equation (3.2-3) for $d\kappa$ with the already coupled flow and kinematic hardening equations given in equation (3.2-7a) and equation

(3.2-5), respectively. Therefore, computational methods for use in plasticity solutions must be selected that appropriately account for the coupling effects. This selection process is not within the scope of this model.

In general, the kinetic equation given in equation (3.2-3) does not represent a total differential (L , N , and M are independent and are not related as the partial derivatives $\partial\kappa/\partial\varepsilon^C$, $\partial\kappa/\partial\varepsilon^P$, and $\partial\kappa/\partial T$). Also, it is not possible to write $\kappa = \kappa(\varepsilon^C, \varepsilon^P, T)$ independent of the path followed in the $(\varepsilon^C, \varepsilon^P, T)$ space. Nevertheless, N can be determined completely on the basis of isothermal continuous cycling tests (where $d\bar{\varepsilon}^C = dT = 0$). In these tests, κ at any ε^P is given as $\kappa = \kappa_0 + \int \varepsilon_0^P \cdot N d\bar{\varepsilon}^P$.

Concerning the nature of the L and N scalar functions in equation (3.2-3), it can be seen that these are inelastic modulus-like quantities in that they relate the change of κ (characterising the yield surface) to the change of inelastic strain. During isothermal plastic loadings for which creep effects are negligible, it can be seen that the N value controls the proportion of isotropic to kinematic hardening. Choosing $N = C \cdot \sqrt{3 \cdot \kappa}$, for illustration, would produce $d\alpha_{ij} = 0$, turning the model into a pure isotropic hardening model, and choosing $N = 0$ would turn the model into a pure kinematic model. Thus, for combined isotropic-kinematic hardening effects, the range of N should be $C \cdot \sqrt{3 \cdot \kappa} > N > 0$.

Experimental data from uniaxial cyclic elastic-plastic tests (with and without hold periods) indicate that N has a strong functional dependence on accumulated inelastic strain (or work). $N/\sqrt{3 \cdot \kappa}$ takes on maximum values by usually between $0.10 \cdot C$ and $0.25 \cdot C$ for the virgin material condition. As cycling progresses, N diminishes with accumulated strain reaching essentially a zero value at loop saturation. For SSs of types 304 and 316, saturation occurs with inelastic strain accumulations of the order of unity (100 %). Not enough is known to generally quantify N due to all effects (including time, temperature, and cyclic frequency).

Available experimental data suggests that prior creep (time dependent) deformations have much the same hardening influence on subsequent cyclic elastic-plastic behaviour as do accumulated plastic strains. Therefore, the recommended procedure is to set $L = N$ so that equation (3.2-3) reduces to:

$$d\kappa = N \cdot (d\bar{\varepsilon}^C + d\bar{\varepsilon}^P) + M \cdot dT \quad (3.2-14)$$

Available data suggests that $d\kappa$ can be alternatively expressed in terms of inelastic work as follows:

$$d\kappa = N^* \cdot (dW^C + dW^P) + M \cdot dT, \quad (3.2-15)$$

where $N^* = N/\sqrt{3 \cdot \kappa}$, and:

$$dW^C + dW^P = \sigma'_{ij} : (d\varepsilon_{ij}^C + d\varepsilon_{ij}^P) \quad (3.2-16)$$

is the increment of inelastic work due to creep and plastic strains.

It is recommended that for SSs of types 304 and 316, the following relation for N be used:

$$N = 0.0022 \cdot (E/C)^{1.3} \cdot C \cdot \sqrt{3 \cdot \kappa_0} \cdot \exp(-0.04 \cdot I), \quad (3.2-17a)$$

where inelastic strain, I , in unit of percent is defined as:

$$I = \int d\bar{\epsilon}^C + \int d\bar{\epsilon}^P \quad (3.2-17b)$$

and $d\bar{\epsilon}^C$ and $d\bar{\epsilon}^P$ are increments of effective creep and plastic strain, respectively. This expression for N captures, through the exponential, the decaying rate of the isotropic hardening, and it generally can elevate the hardening κ value beyond κ_{\max} . To do this more quickly and simply, yet systematically, it is recommended to use the following constant maximum value:

$$N_{\max} = 0.25 \cdot C \cdot \sqrt{3 \cdot \kappa_0}, \quad (3.2-17c)$$

be used. In a simple monotonic loading this means that one-fourth of the plastic hardening will result in isotropic hardening, and the other three-fourths go to kinematic hardening.

Selection of κ_{\max}

As previously mentioned, κ_{\max} should usually be taken as κ_1 obtained from the tenth cycle stress-strain loop of a continuous cycling test. The tenth cycle loop is a compromise to approximately account for the softening effect of high temperature hold periods on the fully hardened material. Use of κ_1 would be appropriate, for example, for analysing cycles separated by long hold periods (several days). In cases where hold times are not long and the strain range is small ($< 0.5\%$) a κ_{\max} value larger than κ_1 is appropriate. The following is recommended:

$$\kappa_{\max} = 0.7 \cdot \left[\kappa_1 \cdot \left(\frac{2}{1 + 0.4 \cdot \Delta\epsilon} \right)^2 \right] \quad (3.2-18)$$

where $\Delta\epsilon$ is the strain amplitude in a uniaxial test. The quantity in brackets represents the saturated κ from continuous cycling stress-strain tests. The 0.7 accounts for some softening that will always occur due to high temperature exposure.

Thermoplastic Effect

The scalar function M in equation (3.2-3) controls the rate of change of yield with temperature during non-isothermal loadings. It should be noted that yielding is path dependent. Thus, while M has been observed to be of the same order as $\partial\kappa_0/\partial T$ (the temperature dependence of initial yield), it is not totally appropriate to use the latter in a non-isothermal analysis. Rather, special non-isothermal tests are required to determine M . A limited number of such tests have been performed on SSs of types 304 and 316 and they show that although M , like N , is a decreasing function of accumulated inelastic strain, it can be approximately represented by a constant.

In the absence of more definitive information, the following definition of M is recommended:

$$M = -0.5 \cdot \alpha_T \cdot C \cdot \sqrt{3 \cdot \kappa_0} \quad (3.2-19)$$

where α_T is the coefficient of thermal expansion. In determining M , which is only mildly temperature dependent, α_T , C and κ_0 values for some representative mean temperature should be used. This procedure is in keeping with the approximate nature of M .

On implementation of ORNL material model in Abaqus

For kinematic work hardening, Ziegler's hardening rule [15] is used in Abaqus [13], as generalized to the non-isothermal case. The Nuclear standard NE F9-5T [14] provides for some coupling between the plasticity and creep responses by allowing prior creep strain to expand and translate the subsequent yield surface in stress space. For SSs of types 304 and 316, however, prior plasticity does not change the subsequent creep response.

3.3 Numerical heat transfer and stress/strain simulations

The prepared FEM model is presented in the following, together with the associated boundary conditions. This follows with a presentation of the performed heat transfer and stress/strain FEM simulations.

All heat transfer and stress/strain analyses were performed with FEM code Abaqus, version 6.8-2 [12, 13]. Concerning the analysis steps loading of WRSs and Start of operation that include both mechanical and temperature loads, they were performed as fully coupled. This means that the heat transfer and stress/strain solutions were obtained from the same analysis run. As for analysis steps corresponding to analysis case specific load cycle sequences with altering mechanical loads but constant temperature, they were performed as static stress/strain analyses. To summarise, for each analysis run the first two steps were performed as fully coupled and the rest as static.

With Abaqus the time incrementation in a transient heat transfer analysis can be controlled directly by the user or automatically by the analysis code. Automatic time incrementation is generally preferred [13]. However, here due to the selected fully coupled analysis type, only user predetermined incrementation is allowed by the analysis code. This is carried out as a function of time, so that for each analysis step a suitable time increment is selected, i.e. these increments are analysis step specific. For analysis steps loading of WRSs and Start of operation, with corresponding durations of 3000 and 27000 s, the selected time increment for both was 50 s.

As for static analysis steps in the performed analyses, i.e. the load cycle sequences with total duration of 30000 s in each case, the maximum allowed time increment was 25 s. And as an ending criterion the analyses were continued keeping as static conditions those with which the last load cycle ended until the stress distributions had ceased altering, which took at maximum 1000 s, depending of the case.

For all analysed components the stress free temperature in the stress analyses was chosen as 286 °C, for justifications see e.g. reference [16]. In the Abaqus analyses this is included in the analyses in the form of so called reference temperature, which is related to the stress free temperature.

With load type Body Force of Abaqus it was possible to create such a stress field in the safe-end/pipe joint weld region of the FEM model that after continuing the analysis step loading of WRSs to steady state in the preparatory analyses the result was a somewhat correct locally confined WRS distribution, both concerning maximum and minimum values and distribution shape. However, this took several attempts. With load type Initial stress of Abaqus this was not possible, as explained in the previous project report [3].

To improve convergence in the FEM analyses, the line-search technique was used. With this technique one obtains a direction from an iterative procedure such as full and modified Newton-Raphson iteration [17]. The advantage in this technique is that by solving only a one-dimensional problem a better approximation is obtained. Then also the computation times of the analysis runs become shorter. Moreover, in some cases when it was not possible to achieve convergence with any other available means, it finally succeeded with the line-search technique.

It was deemed that 50 LCs in each prepared load history would suffice to show how the WRSs change/decrease as a function of LCs in the FEM simulations, if at all. This selected number of covered load cycles was also based on the computational feasibility, because as each load history was incorporated to a single analysis run, it was noticed in the preliminary analyses that the size of the output files soon became relatively large, i.e. of the scale of several GBs. With the selected number of analysis run specific load cycles the size of the output files and the analysis run durations stayed reasonable. Here a 2.0 GHz PC having two CPUs and 2.0 GB of RAM memory was used.

The main results from the heat transfer and stress/strain analyses are presented in Section 3.4.

3.3.1 Boundary conditions

The thermal and displacement boundary conditions of the FEM model of the examined safe-end, pipe and their joint weld, used in the fully coupled heat transfer and stress/strain analyses, are described in the following.

The thermal boundary conditions of the FEM model of the examined safe-end, pipe and their joint weld are the following:

1. The outer surfaces, see Figure 3.3.2-1, are insulated and the heat transfer through the isolation is insignificant as compared to the heat transfer caused by the considered loads. Therefore an adiabatic boundary condition was applied, i.e. $\alpha_{HT} = 0 \text{ W/m}^2\text{K}$.
2. At the cut-off sections at the safe-end and pipe ends, see Figure 3.3.2-1, no heat exchange will exist that influence the examined phenomena, i.e. in both surfaces the heat transfers to in and out directions are equal, and thus cancel each other. Therefore an adiabatic boundary condition was applied, i.e. $\alpha_{HT} = 0 \text{ W/m}^2\text{K}$.
3. At the inner surfaces, see Figure 3.3.2-1, heat will be exchanged between water and metal. The amount of heat that will be exchanged is controlled by the heat transfer coefficient α_{HT} , and its values vary between 1000 and 70000 $\text{W/m}^2\text{K}$.

The displacement boundary conditions of the examined safe-end and pipe are the following:

1. At the safe-end side vertical cut-off surface, see Figure 3.3.2-1, the horizontal displacements are set to zero. Thus the model is horizontally fixed in this plane.
2. At the pipe side vertical cut-off surface, see Figure 3.3.2-1, the model is exposed to loads from the piping, which are described in Section 3.1.3. This surface is set to remain vertical and straight, but allowed to deform perpendicular to itself.
3. Due to the characteristics of the selected model type, i.e. axisymmetric, the deformations are in practise two dimensional, as in radial and longitudinal directions they are the same for each section parallel to the symmetry axis of the model.

3.3.2 FEM model

As all considered loads, including WRS distributions, are symmetric in relation to geometry symmetry axis of the examined safe-end, pipe and their joint weld, it was sufficient to prepare an axisymmetric FEM model for the needed numerical simulations. The element mesh used for the examined safe-end, pipe and their joint weld is shown in Figures 3.3.2-1 and 3.3.2-2. As mentioned earlier, this is the same FEM model that was created during 2008 works of the project.

In the direction of the model symmetry axis, being y-axis in the two figures in question, the length of the FEM model is approximately 750 mm. In general, the geometry of the analysed components and material property data of the associated materials needed to create the FEM model are presented in Sections 3.1.1 and 3.1.2, respectively. The loads acting on the FEM model are presented in Section 3.1.3.

As can be seen from Figures 3.3.2-1 and 3.3.2-2, the number of elements through the wall in the model is 16, so in that direction in the safe-end/pipe joint weld region the length of the elements is quite accurately 1.0 mm. The side lengths of the elements varied between 1 to 13 mm in the model, with smallest element size and highest density in the region of the examined safe-end/pipe joint weld.

The axisymmetric FEM model was meshed with general purpose continuum elements. The selected element type from the Abaqus element library is CAX4RT, which is a 4-node rectangular bilinear displacement and temperature element, with reduced integration and hourglass control. Active degrees of freedom are the two displacements in the model plane, i.e. in the vertical (x-axis) and horizontal (y-axis, being here also the FEM model symmetry axis) directions, and temperature. The number of the nodes and elements in the model are 2836 and 2650, respectively.

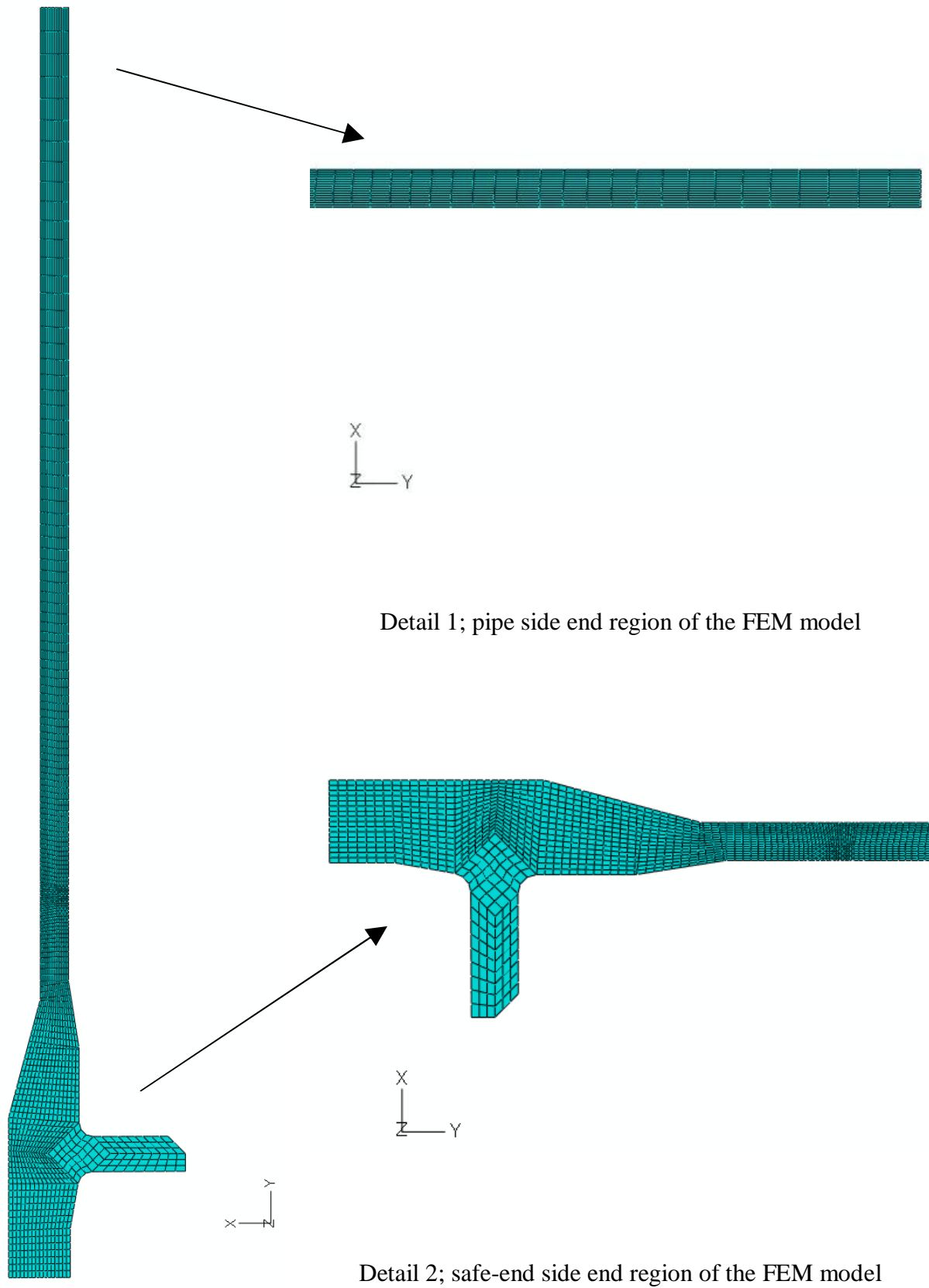


Figure 3.3.2-1. The overall element mesh and two mesh details of the axisymmetric FEM model of the examined safe-end, pipe and their joint weld.

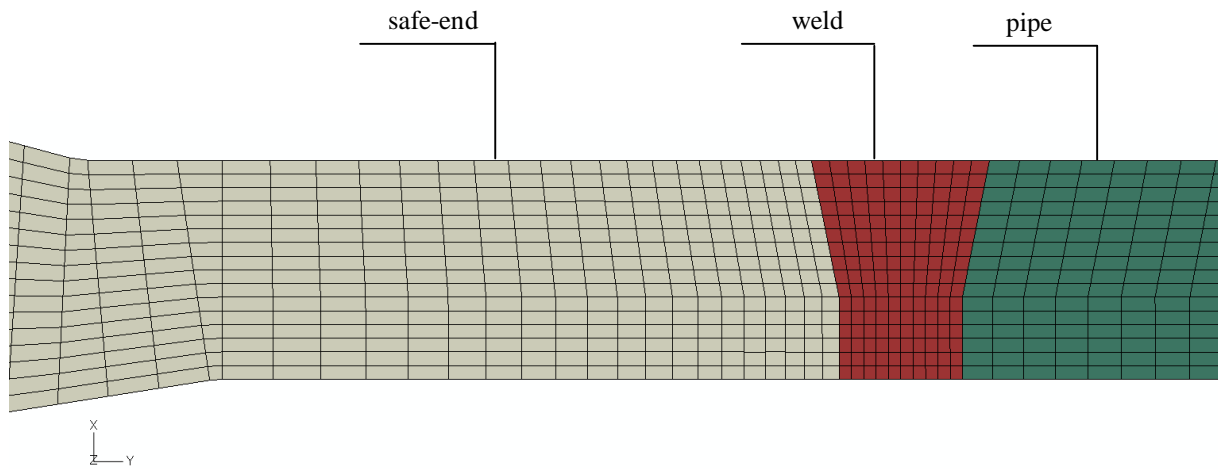


Figure 3.3.2-2. Detail of the element mesh of the axisymmetric FEM model of the examined safe-end, pipe and their joint weld, showing all involved material regions emphasised with different colours. For the location of this detail in the complete element mesh, see Figure 3.3.2-1.

3.4 WRS simulation results

In the following is a presentation concerning the FEM analysis results. It was decided to limit the presentation here to concern only axial WRSs, as worldwide more than 90 % of the detected piping crack cases have been oriented circumferentially, see e.g. ref. [18], and it is mainly the axial stresses that make such cracks grow.

More specifically, the WRS results obtained with FEM for the safe-end/pipe joint weld are examined in two sets of element mesh nodes, see Figure 3.4-1 in the following. In the through wall direction the spacing of the nodes is even for both node sets. As for the directions of the lines along which the nodes of the two examined node sets are located, the weld centre line (WCL) is vertical, whereas the weld offset line (WOL) tilts slightly from the vertical direction near the middle of the wall.

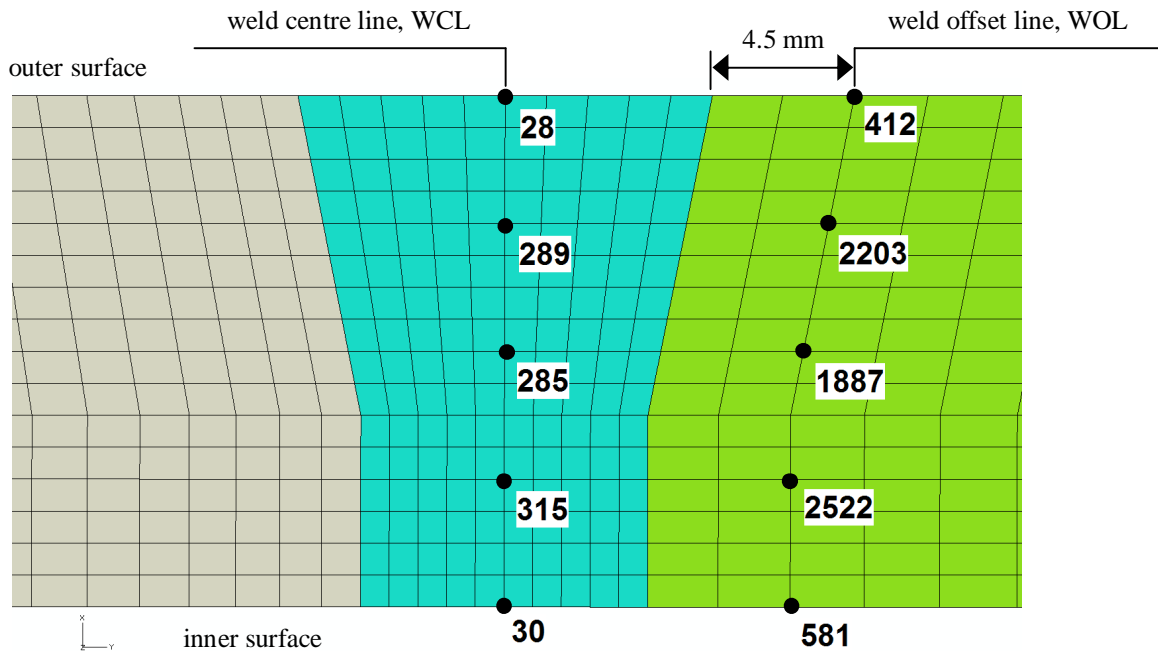


Figure 3.4-1. The node numbers of the two examined node sets in the safe-end/pipe joint weld element mesh region. Both sets are evenly spaced in the through wall direction, with the weld centre line being vertical, whereas the weld offset line tilts slightly near the middle of the wall.

Note that despite the applied means to enhance convergence, analysis case LCS1 still diverged after 10th load cycle, while in the other seven cases the analysis runs converged through the considered load histories.

For the considered load histories the transverse to weld stress results are presented for the safe-end/pipe joint weld centre line as diagrams in Figure 3.4-2 to 3.4-9, and for the weld and to some extent the adjacent material regions as colour surfaces for some selected time instants in Figure 3.4-10 to 4.2.3-18, respectively. Concerning the stress result diagrams the values have been taken from the WCL nodes.

As described earlier and what can be seen from the stress result diagrams, is that the considered eight load histories divide into three main phases, of which the first two are identical to all load histories, while the third one is unique to each load history. Namely, the first phase from 0 to 3000 s is the loading of the WRSs in the overall temperature of 20 °C, and the second phase from 3000 to 30000 s is the load transient called here Start of operation (SO), during which the pressure and temperature are increased to values of 70 bar and 286 °C, respectively. The third phase that is unique to each load history is the considered load sequence, consisting of load sequence specifically constant amplitude load cycles, which are divided here to sets consisting of five cycles, with the duration of each set being 3000 s. Adding up the durations of the first and second phases as well as load sequence specifically those of the ten load cycle sets, results with the total duration of 60000 s for each load history, as can be seen in the stress result diagrams. The exception here is Load history 1 the analysis run of which diverged after the 10th load cycle, and consequently the duration of the presented analysis results in this case cover only 36600 s.

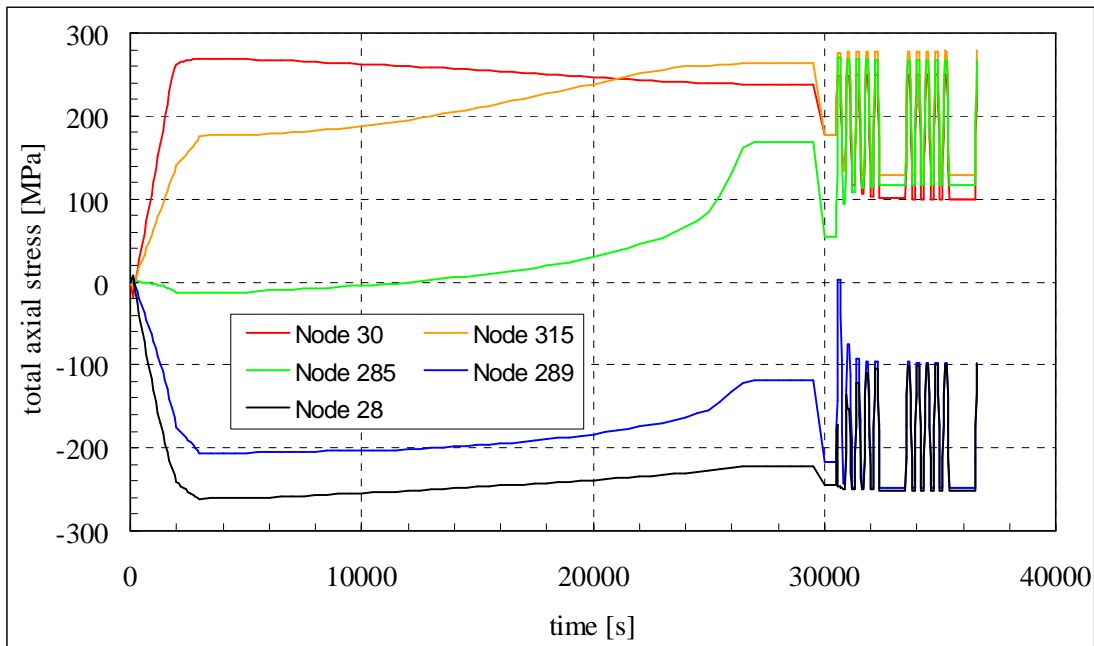


Figure 3.4-2a. The transverse to weld stress results in the safe-end/pipe joint WCL for Load history 1. This analysis case diverged after the 10th load cycle. For details concerning the cyclic loads in question see Table 3.1.3-2 and Figure 3.1.3-1.

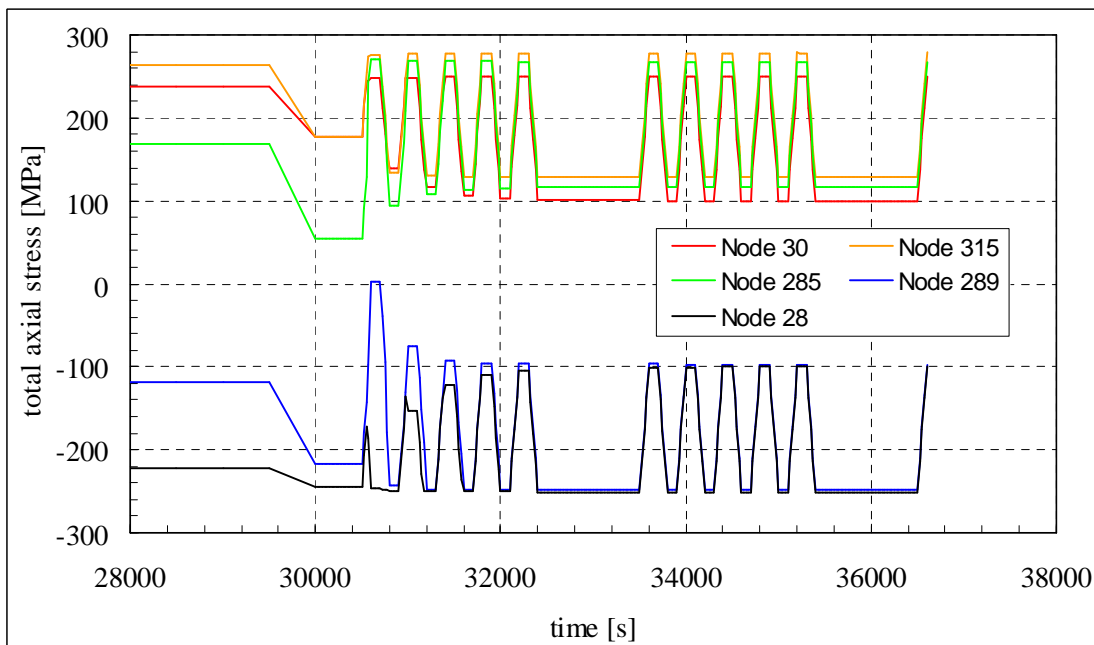


Figure 3.4-2b. Detail of the transverse to weld stress results in the safe-end/pipe joint WCL for Load history 1. This analysis case diverged after the 10th load cycle. For details concerning the cyclic loads in question see Table 3.1.3-2 and Figure 3.1.3-1.

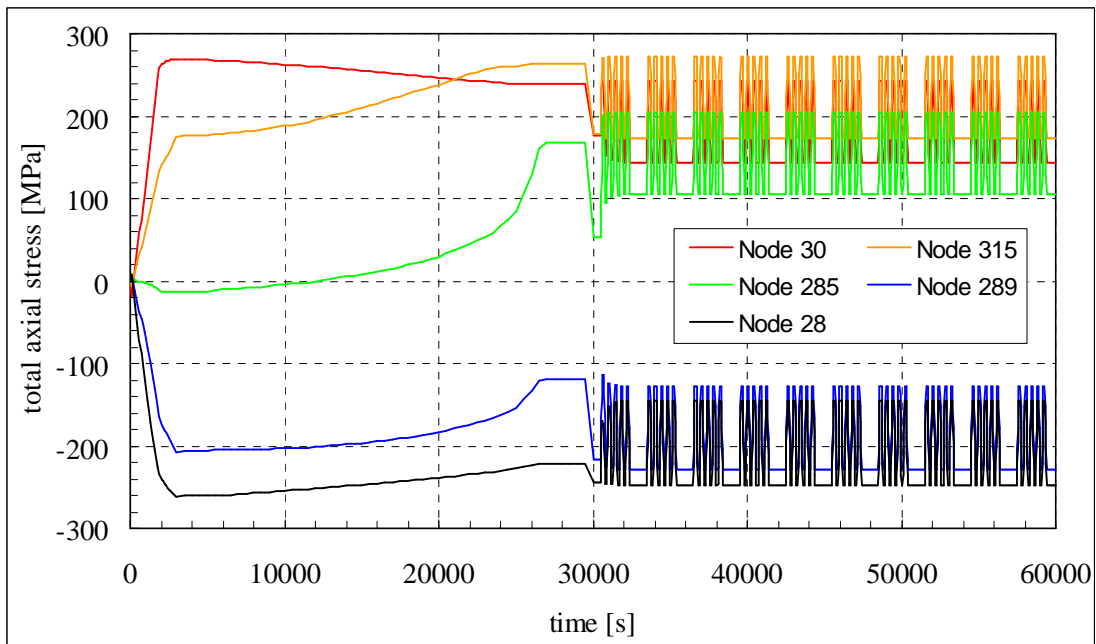


Figure 3.4-3a. The transverse to weld stress results in the safe-end/pipe joint WCL for Load history 2. For details concerning the cyclic loads in question see Table 3.1.3-2 and Figure 3.1.3-1.

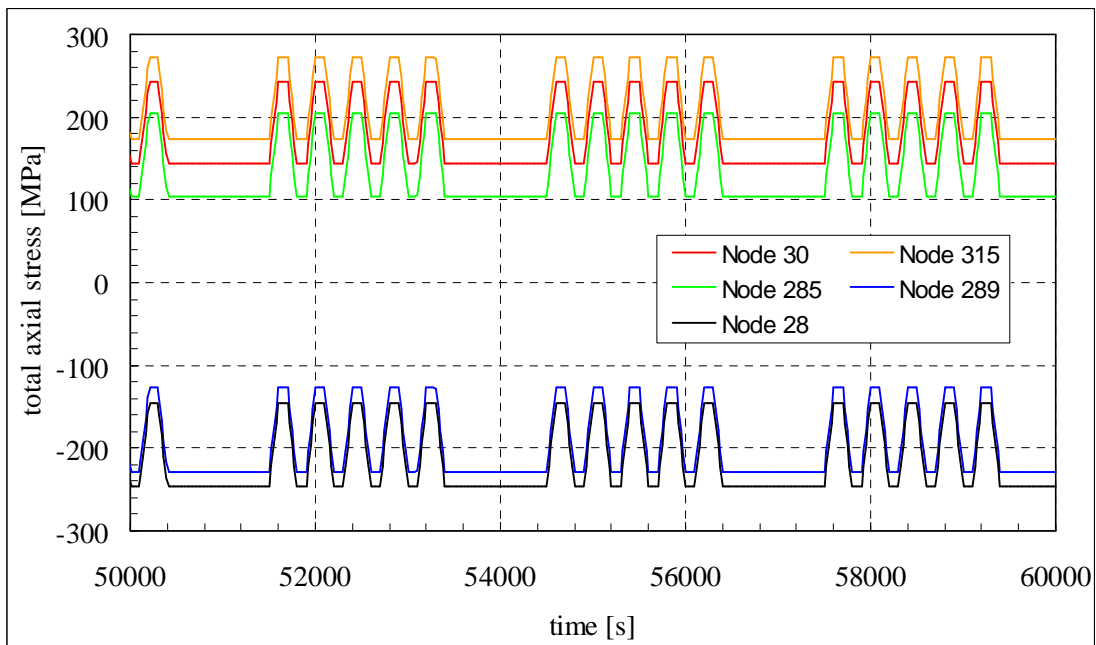


Figure 3.4-3b. Detail of the transverse to weld stress results in the safe-end/pipe joint WCL for Load history 2. For details concerning the cyclic loads in question see Table 3.1.3-2 and Figure 3.1.3-1.

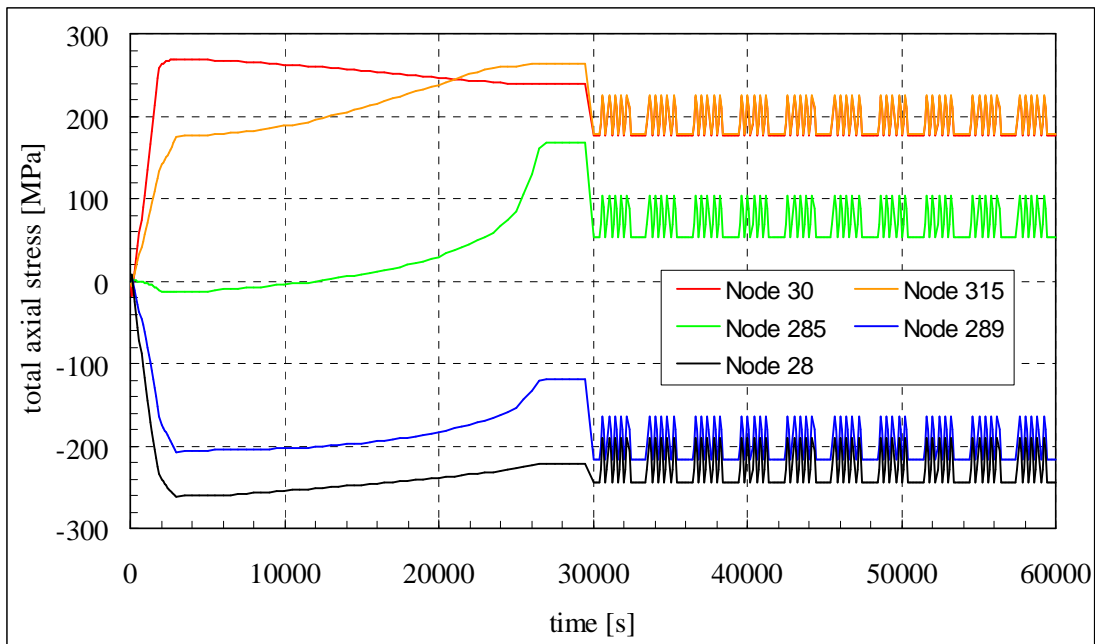


Figure 3.4-4. The transverse to weld stress results in the safe-end/pipe joint WCL for Load history 3. For details concerning the cyclic loads in question see Table 3.1.3-2 and Figure 3.1.3-1.

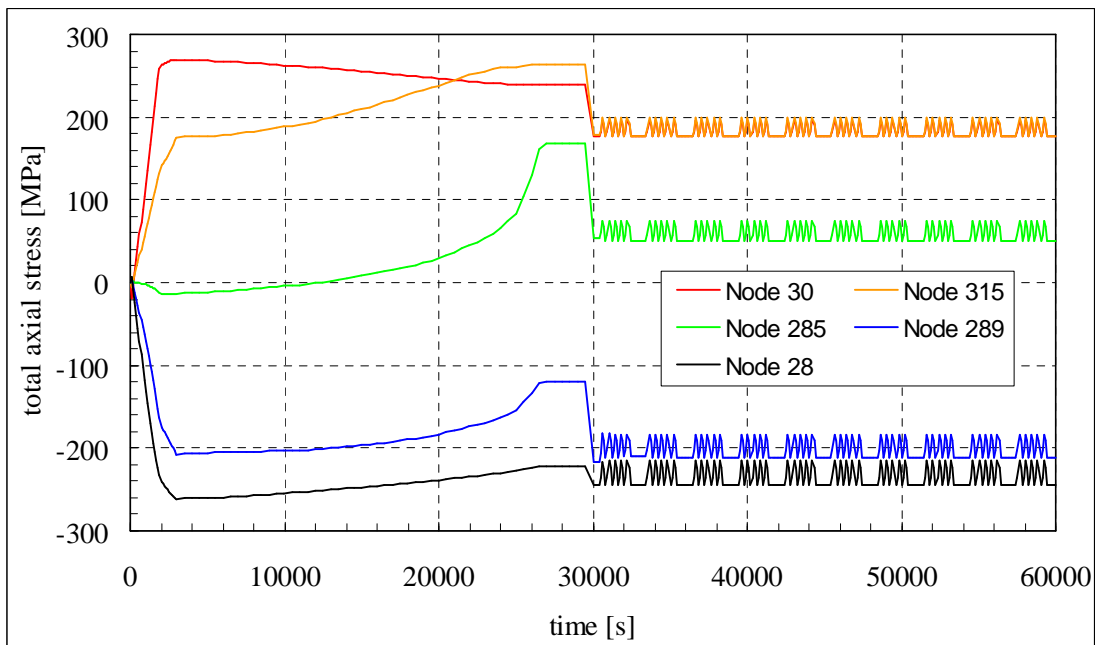


Figure 3.4-5. The transverse to weld stress results in the safe-end/pipe joint WCL for Load history 4. For details concerning the cyclic loads in question see Table 3.1.3-2 and Figure 3.1.3-1.

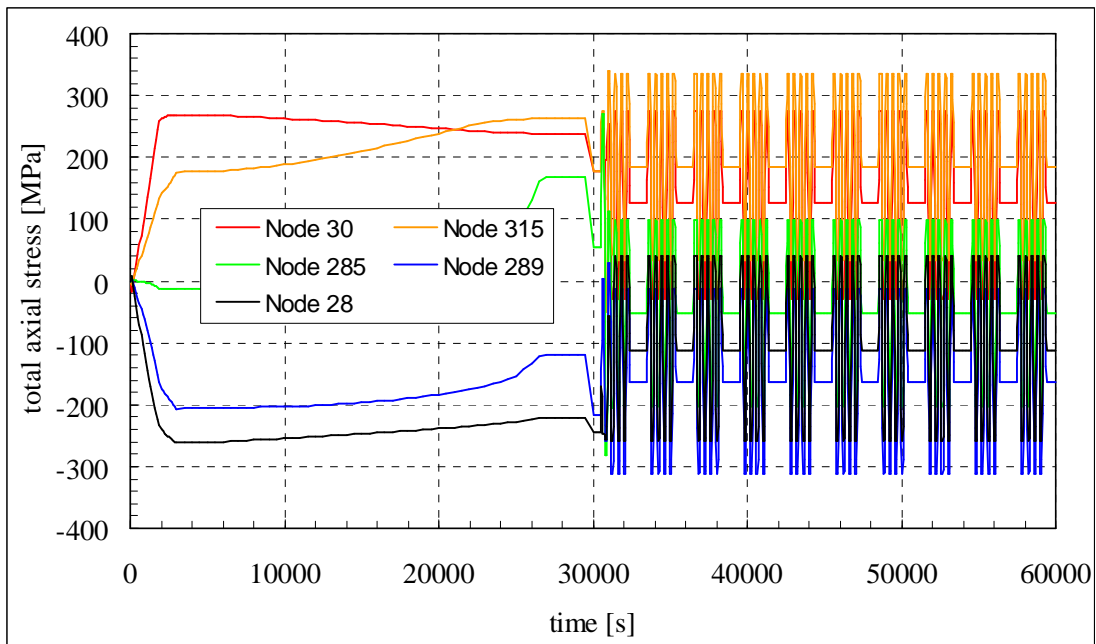


Figure 3.4-6a. The transverse to weld stress results in the safe-end/pipe joint WCL for Load history 5. For details concerning the cyclic loads in question see Table 3.1.3-2 and Figure 3.1.3-1.

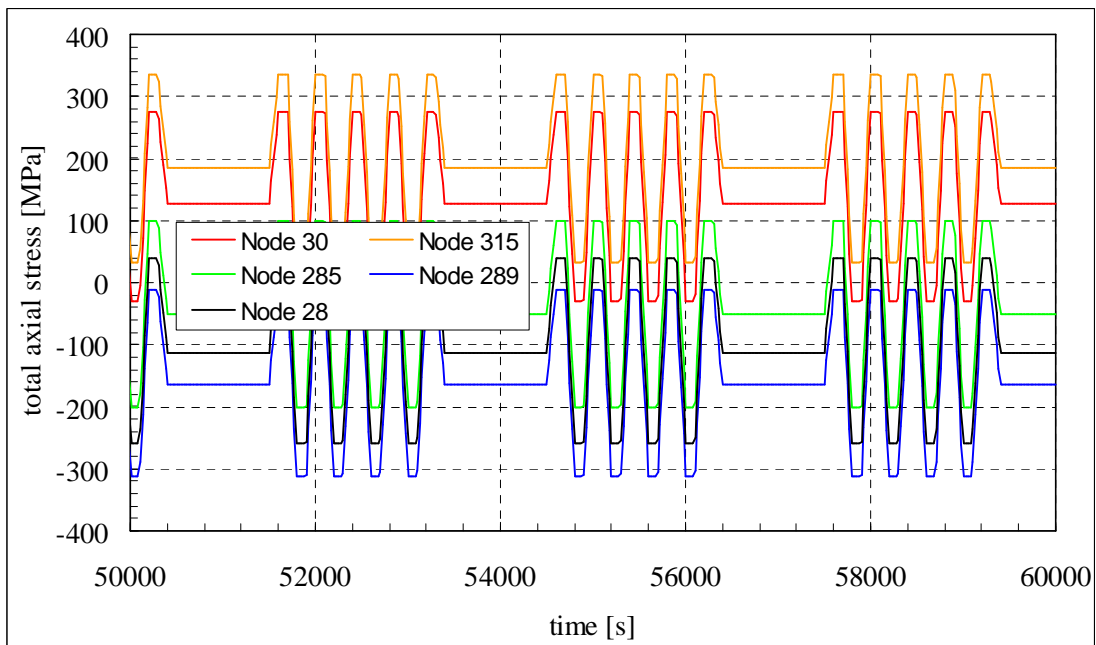


Figure 3.4-6b. Detail of the transverse to weld stress results in the safe-end/pipe joint WCL for Load history 5. For details concerning the cyclic loads in question see Table 3.1.3-2 and Figure 3.1.3-1.

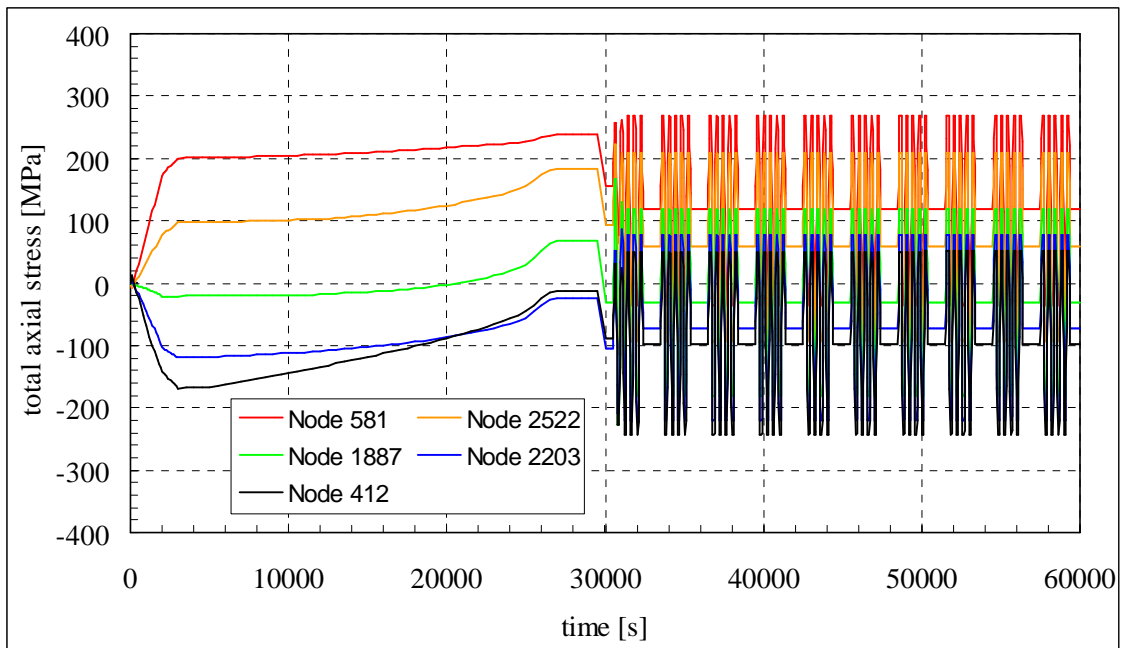


Figure 3.4-6c. The transverse to weld stress results in the safe-end/pipe joint WOL for Load history 5. For details concerning the cyclic loads in question see Table 3.1.3-2 and Figure 3.1.3-1.

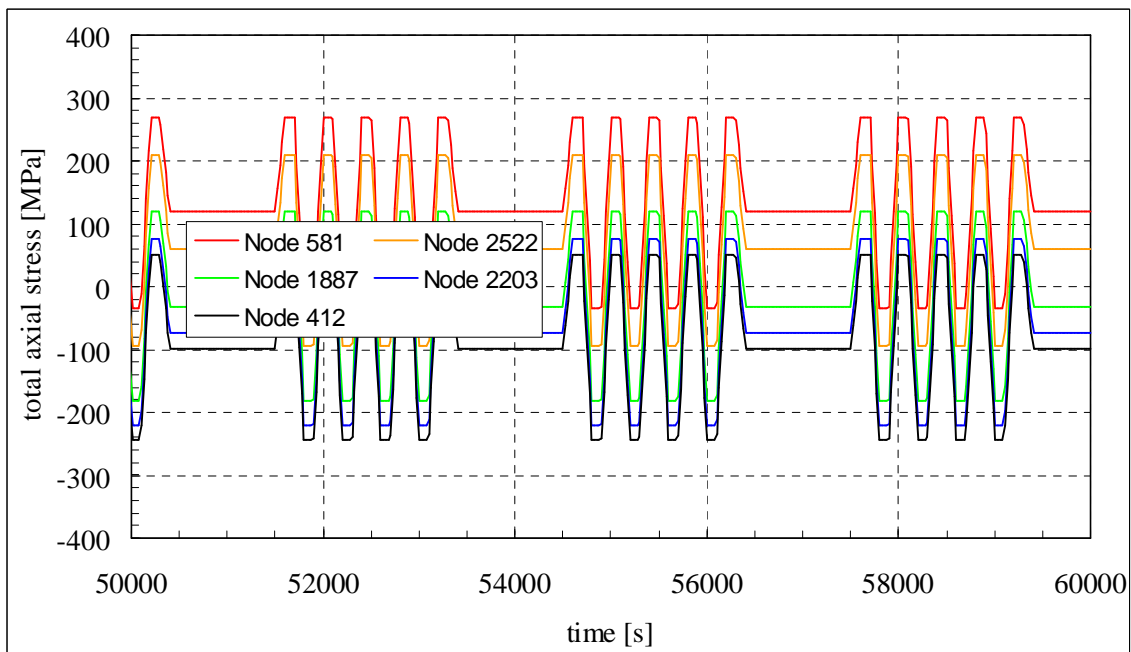


Figure 3.4-6d. Detail of the transverse to weld stress results in the safe-end/pipe joint WOL for Load history 5. For details concerning the cyclic loads in question see Table 3.1.3-2 and Figure 3.1.3-1.

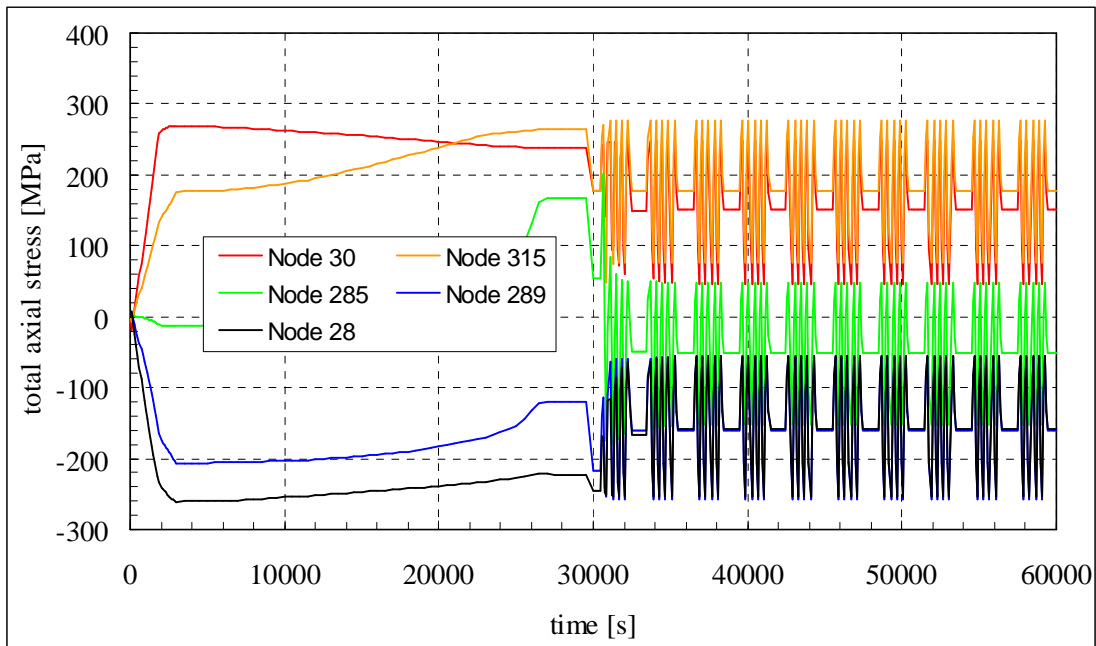


Figure 3.4-7. The transverse to weld stress results in the safe-end/pipe joint WCL for Load history 6. For details concerning the cyclic loads in question see Table 3.1.3-2 and Figure 3.1.3-1.

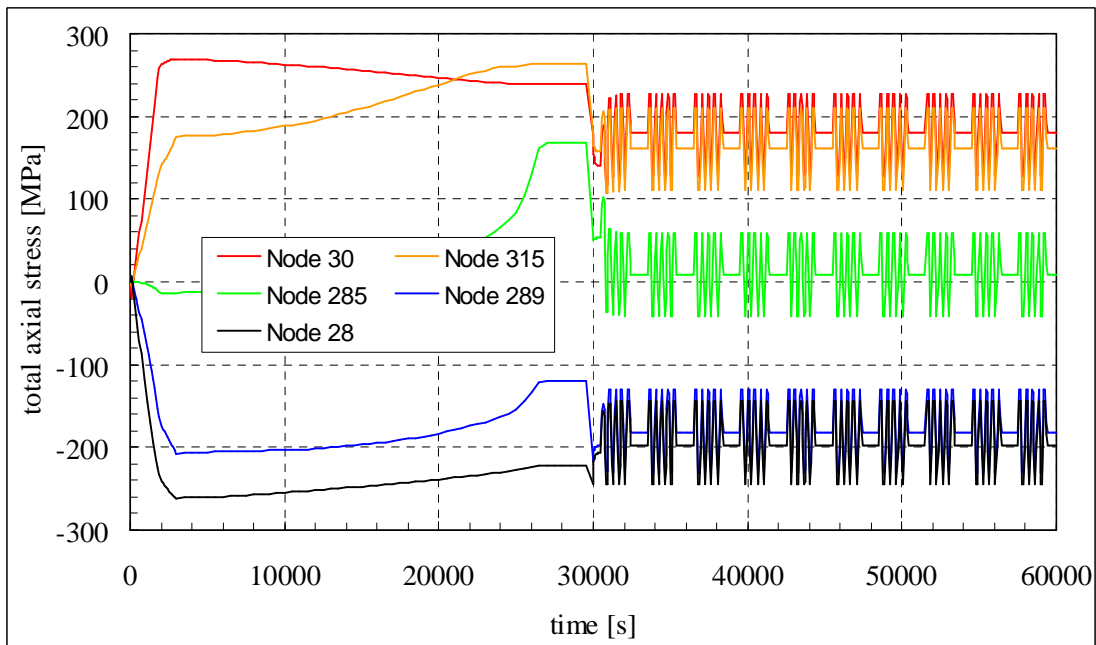


Figure 3.4-8. The transverse to weld stress results in the safe-end/pipe joint WCL for Load history 7. For details concerning the cyclic loads in question see Table 3.1.3-2 and Figure 3.1.3-1.

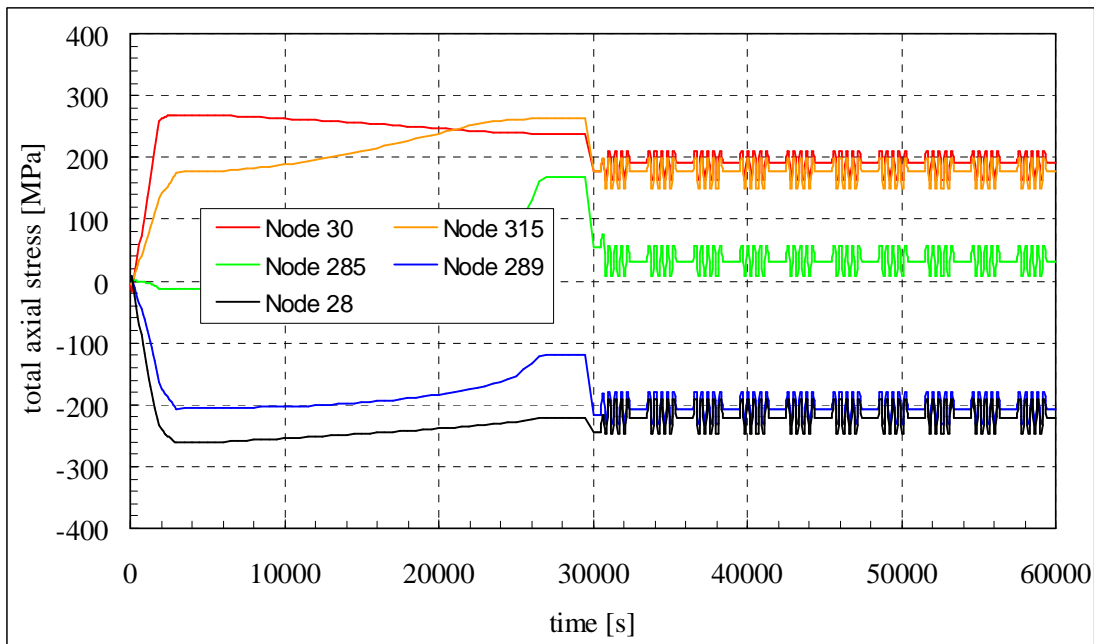


Figure 3.4-9. The transverse to weld stress results in the safe-end/pipe joint WCL for Load history 8. For details concerning the cyclic loads in question see Table 3.1.3-2 and Figure 3.1.3-1.

As mentioned earlier, in the following result figures the total transverse to weld stress results are presented for the safe-end/pipe joint weld and to some extent the adjacent material regions as colour surfaces in some selected time instants from the considered load histories. The first time instant is at the end of the first phase, i.e. loading of WRSs. The following covered time instants are at the end of each considered load history. In addition, for the load histories 1 and 5 which include the most severe cyclic loading phases, are covered also those time instants at which the transverse to weld total stresses reach their maximum values in tension, which occurs during the first or second load cycle of the load cycle sequence phase. In the stress result figures S22 corresponds to the transverse to weld stresses in units of MPa.

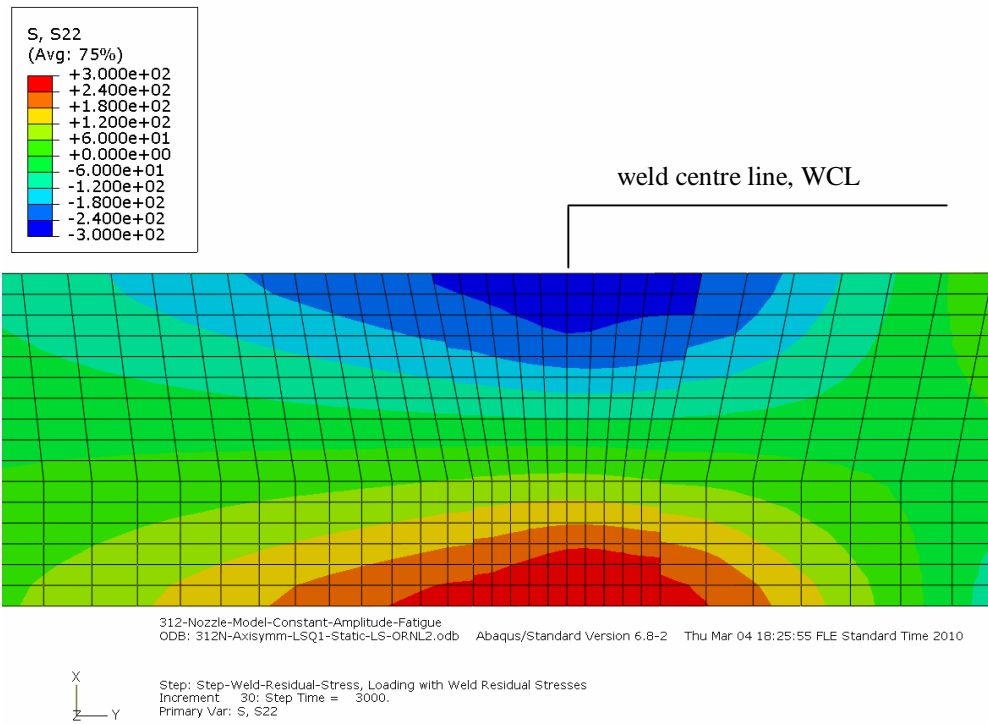


Figure 3.4-10. The transverse to weld stress results for the safe-end/pipe joint at the end of loading of the WRSs; for all considered load histories.

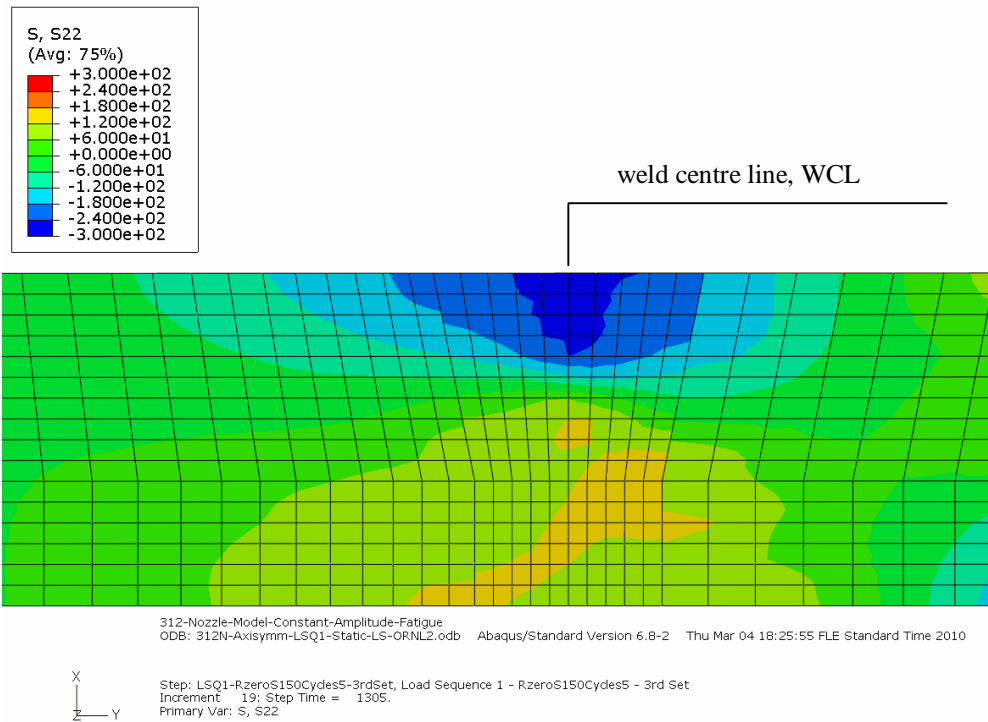


Figure 3.4-11a. The transverse to weld stress results for the safe-end/pipe joint at the end of Load history 1.

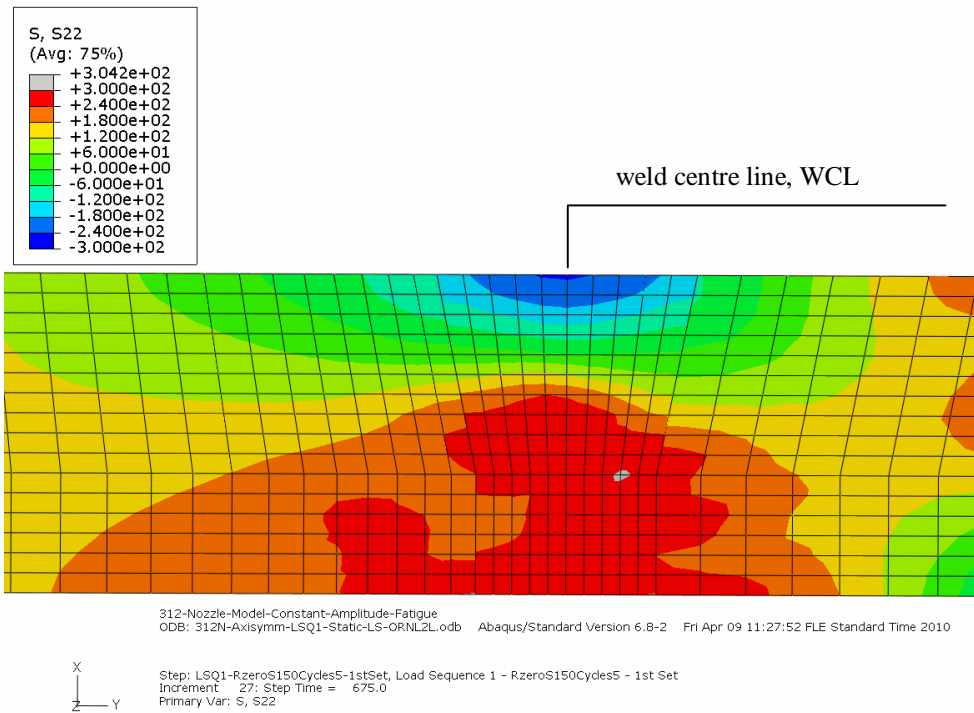


Figure 3.4-11b. The transverse to weld stress results for the safe-end/pipe joint at that time instant they reach maximum values in tension during Load history 1.

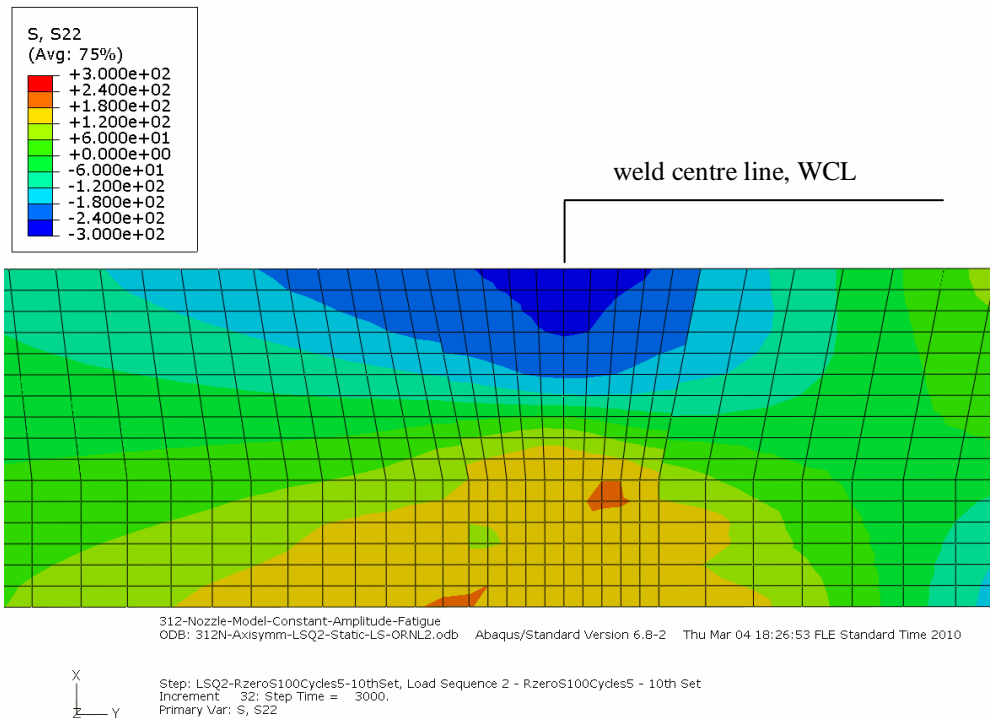


Figure 3.4-12. The transverse to weld stress results for the safe-end/pipe joint at the end of Load history 2.

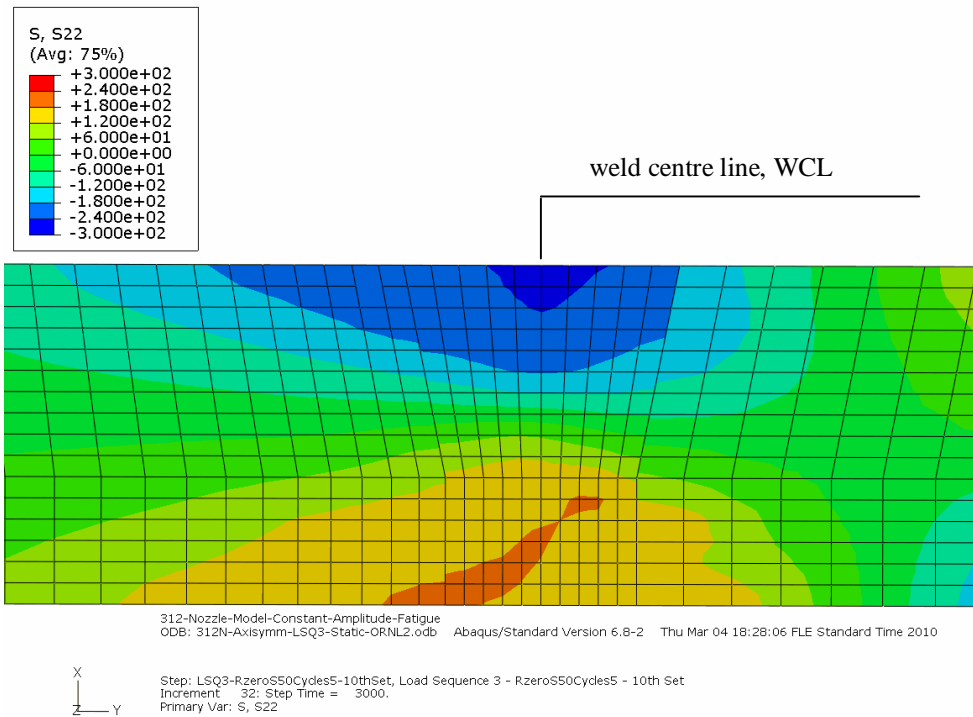


Figure 3.4-13. The transverse to weld stress results for the safe-end/pipe joint at the end of Load history 3.

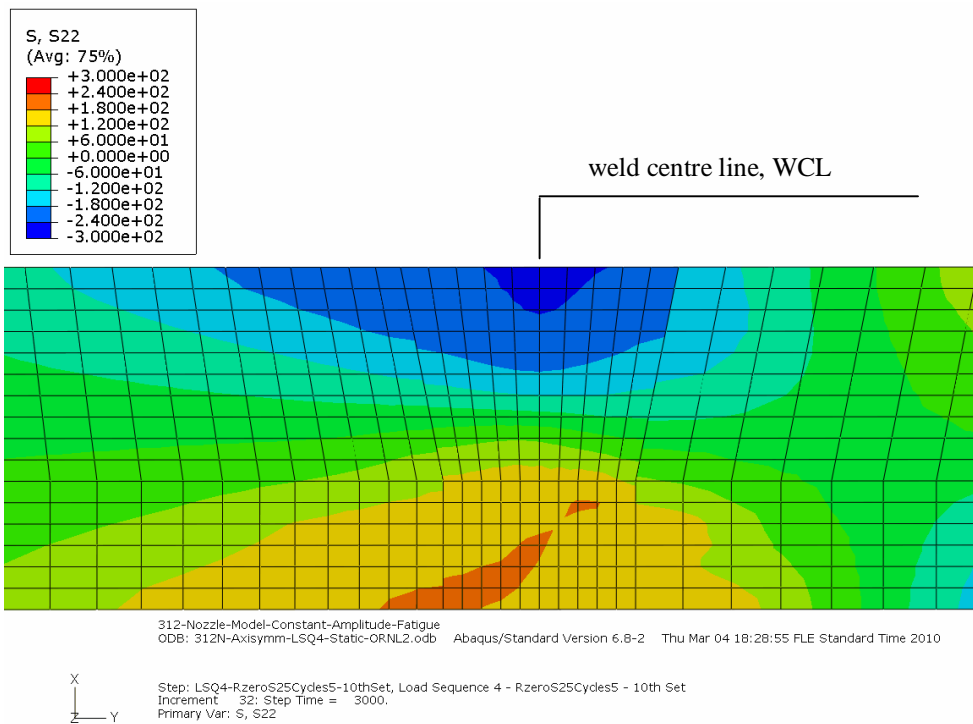


Figure 3.4-14. The transverse to weld stress results for the safe-end/pipe joint at the end of Load history 4.

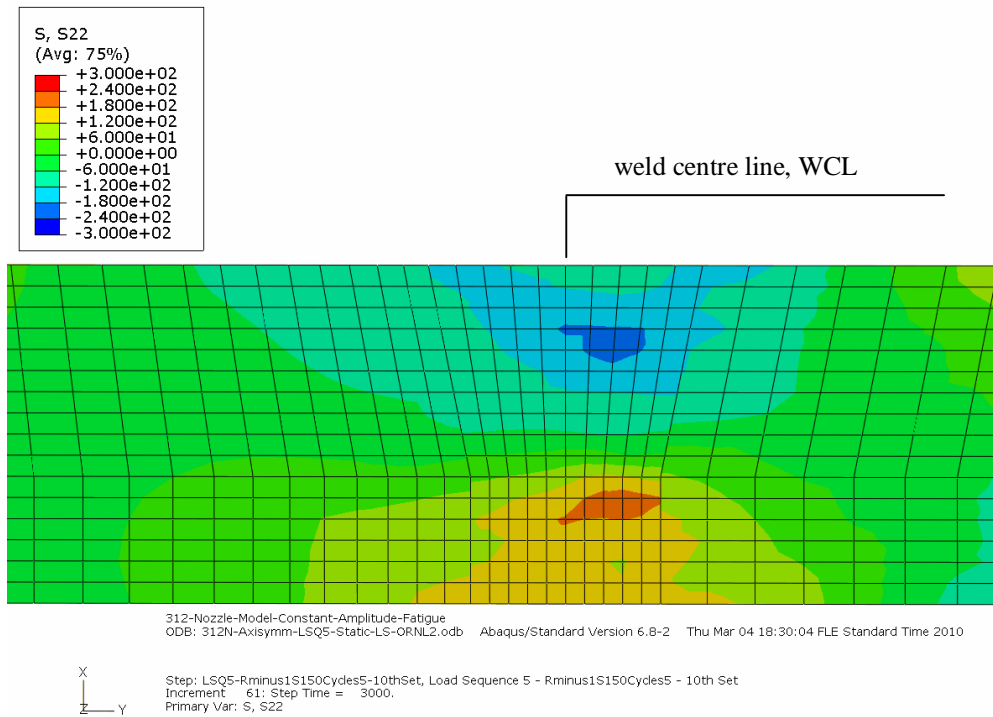


Figure 3.4-15a. The transverse to weld stress results for the safe-end/pipe joint at the end of Load history 5.

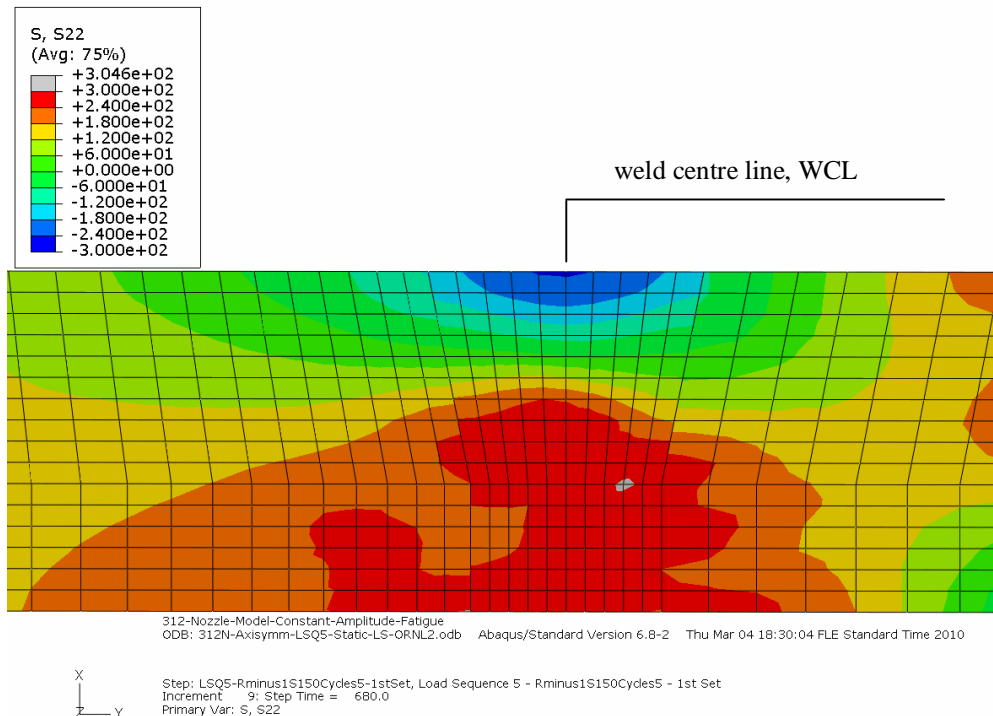


Figure 3.4-15b. The transverse to weld stress results for the safe-end/pipe joint at that time instant they reach maximum values in tension during Load history 5.

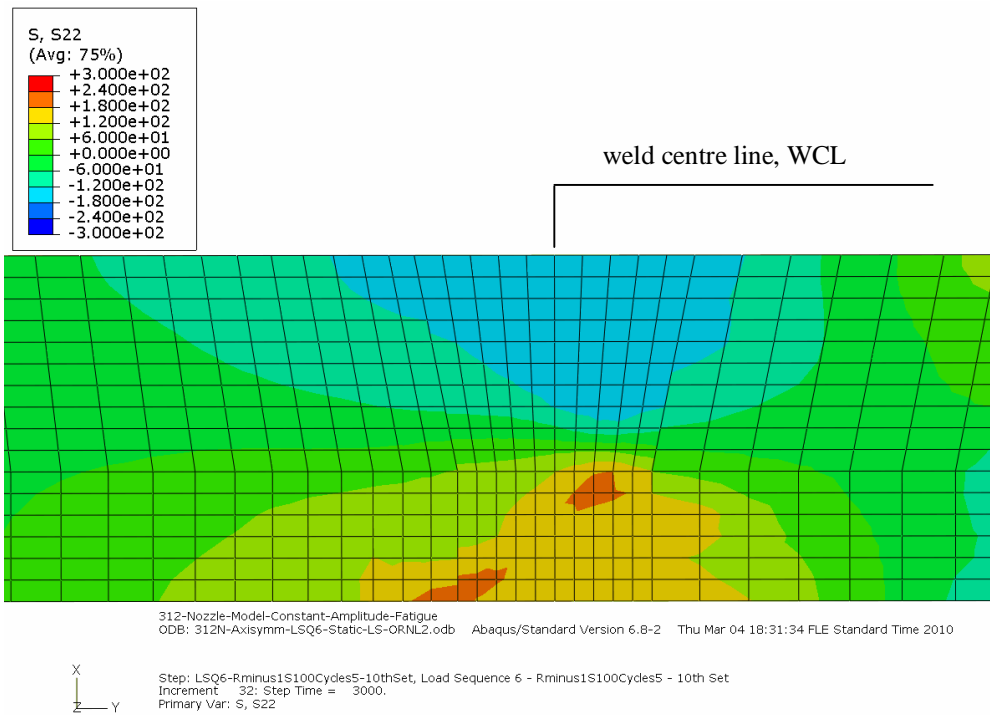


Figure 3.4-16. The transverse to weld stress results for the safe-end/pipe joint at the end of Load history 6.

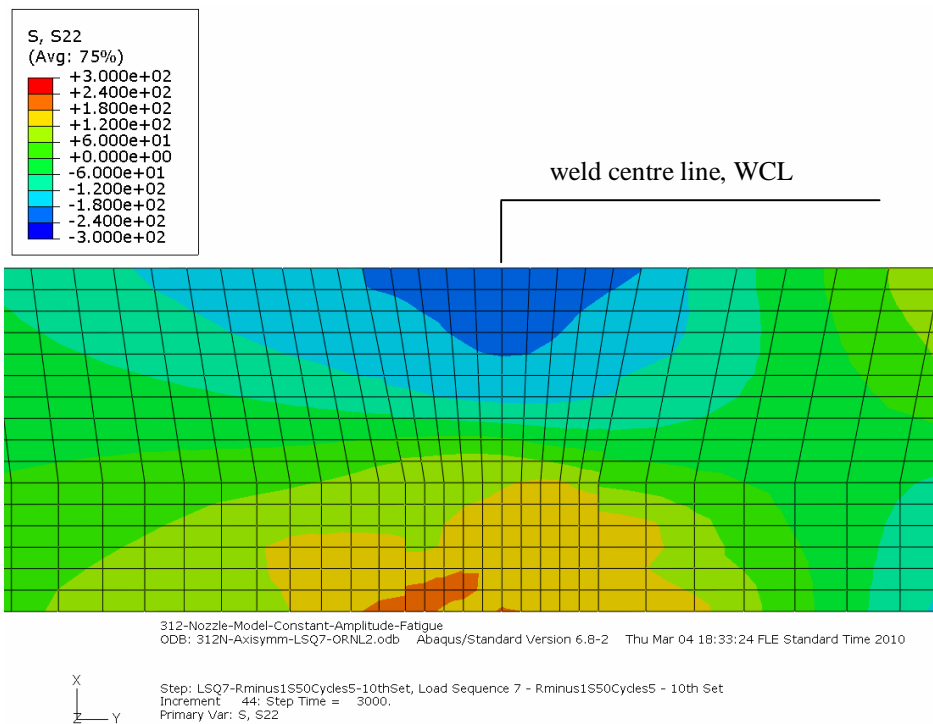


Figure 3.4-17. The transverse to weld stress results for the safe-end/pipe joint at the end of Load history 7.

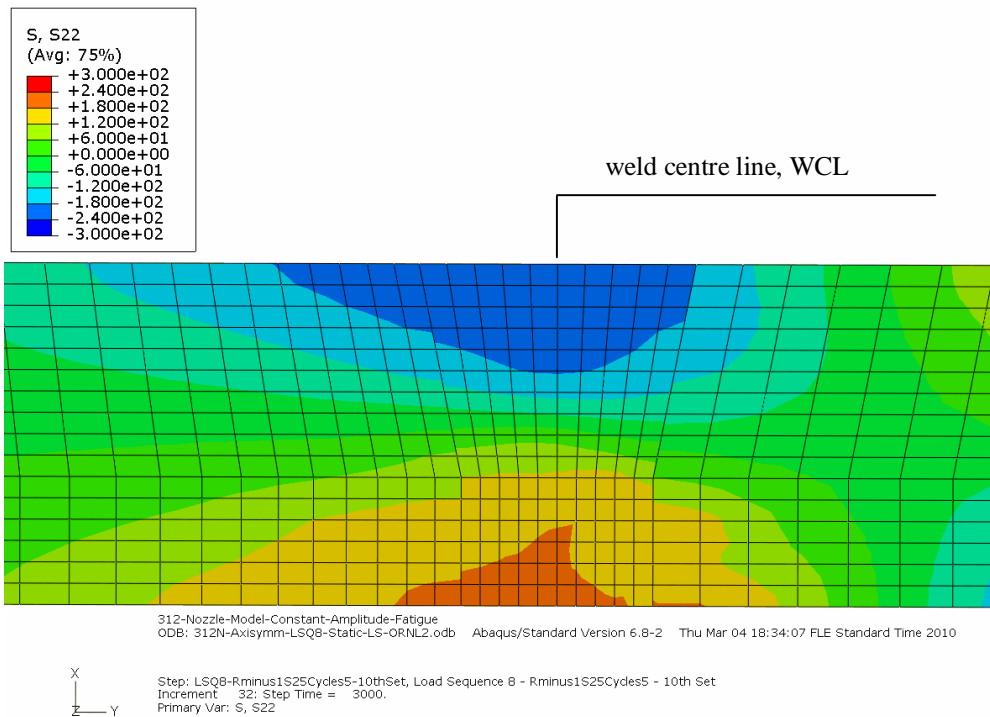


Figure 3.4-18. The transverse to weld stress results for the safe-end/pipe joint at the end of Load history 8.

For some of the considered load histories the transverse to weld stress results are presented as a function of the corresponding strain for the inner and outer surface nodes of the safe-end/pipe joint WCL and WOL in Figures 3.4-19 to 3.4-21. The result examination here is limited to these two node pairs because cross-section specifically they experience the maximum axial stresses in tension and in compression, respectively. Also, only the most severe load histories are considered in this result display selection. It can be seen from these results how it does not take too many cycles for the strain hardening to saturate, i.e. the cyclic curves quite soon cease translating and/or expanding and become quite accurately identical. The anomalies seen in some of these diagrams, meaning those cases were the maximum strain values are approximately two times higher than those of corresponding saturated strain values, concern at most the first five load cycles.

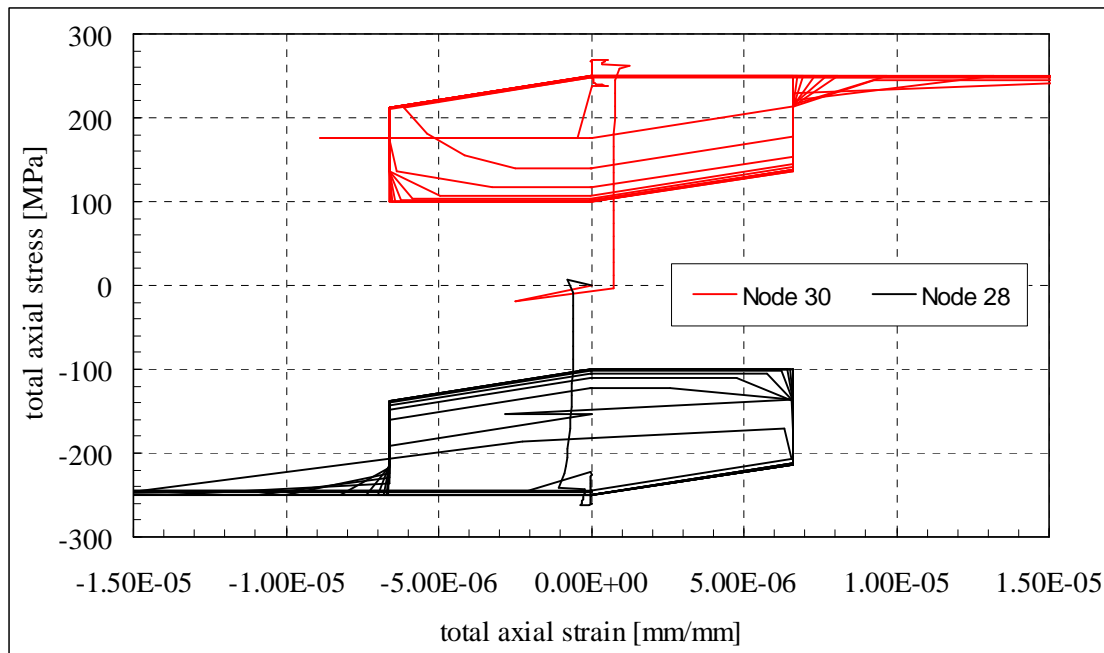


Figure 3.4-19. The total transverse to weld stresses as a function of the corresponding strain for the inner (node 30) and outer (node 28) surface nodes of the safe-end/pipe joint WCL for Load history 1.

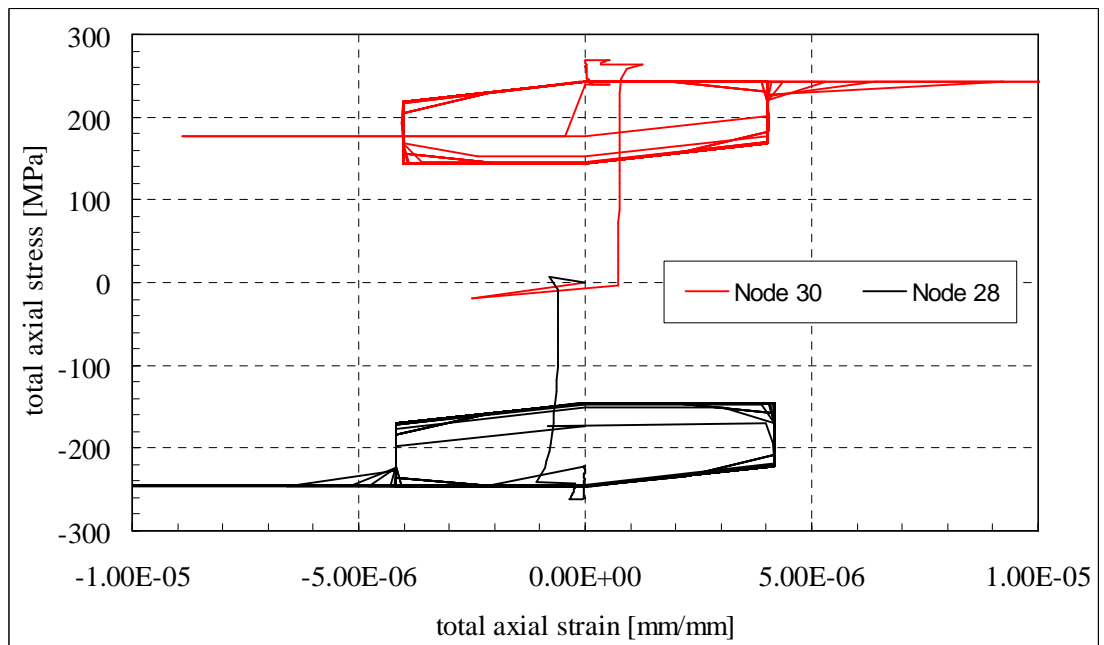


Figure 3.4-20a. The total transverse to weld stresses as a function of the corresponding strain for the inner (node 30) and outer (node 28) surface nodes of the safe-end/pipe joint WCL for Load history 2.

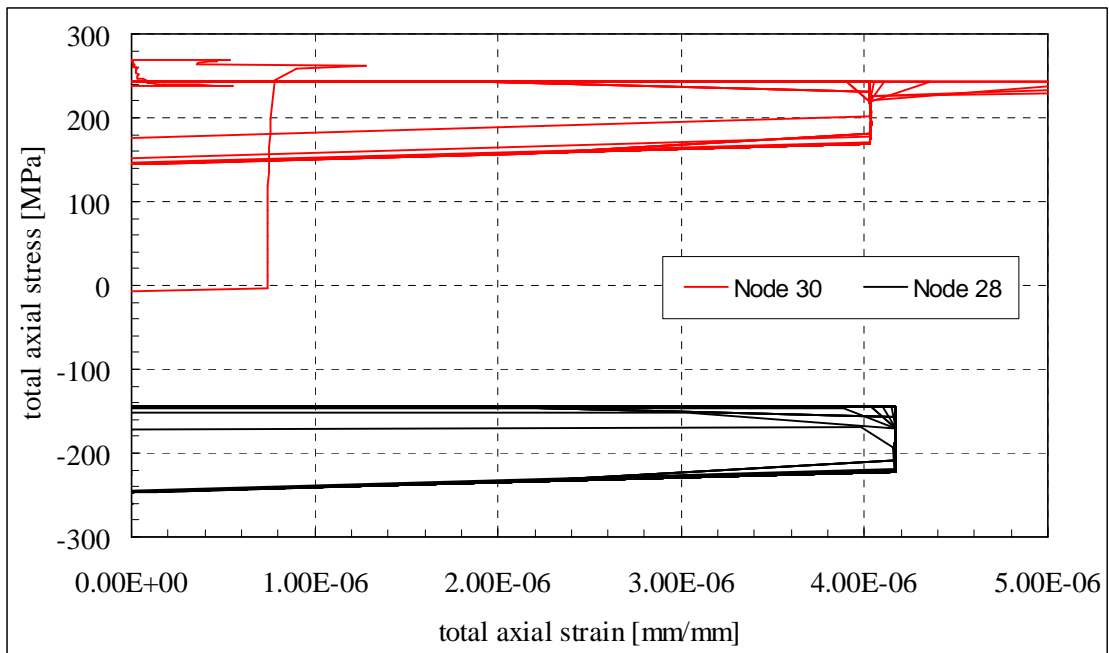


Figure 3.4-20b. Detail concerning the total transverse to weld stresses as a function of the corresponding strain for the inner (node 30) and outer (node 28) surface nodes of the safe-end/pipe joint WCL for Load history 2.

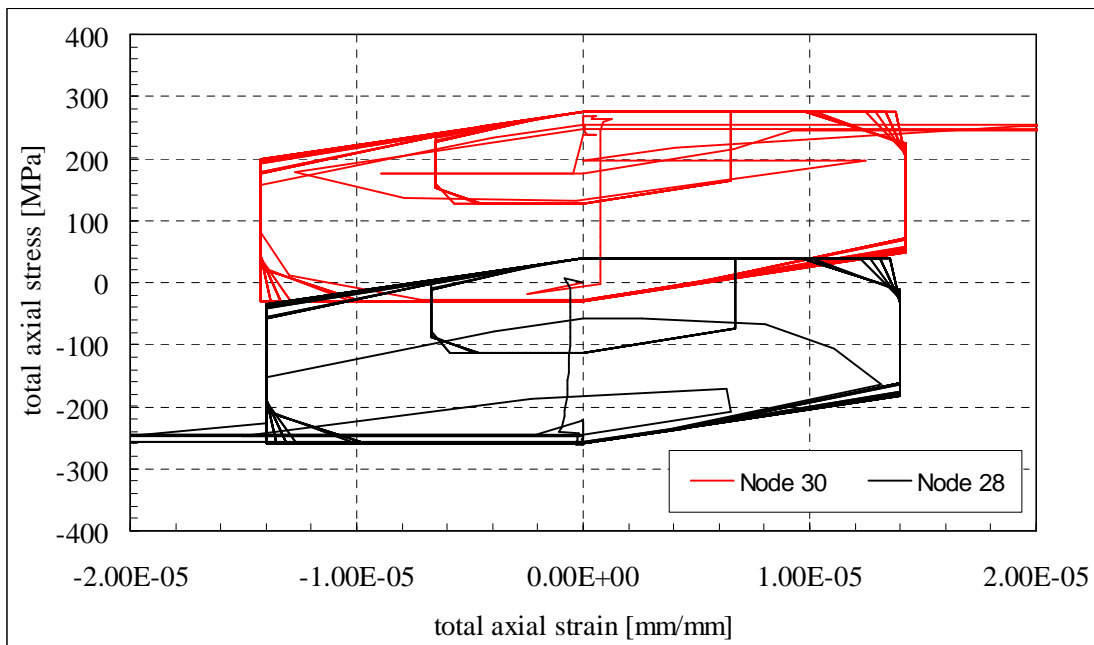


Figure 3.4-21a. The total transverse to weld stresses as a function of the corresponding strain for the inner (node 30) and outer (node 28) surface nodes of the safe-end/pipe joint WCL for Load history 5.

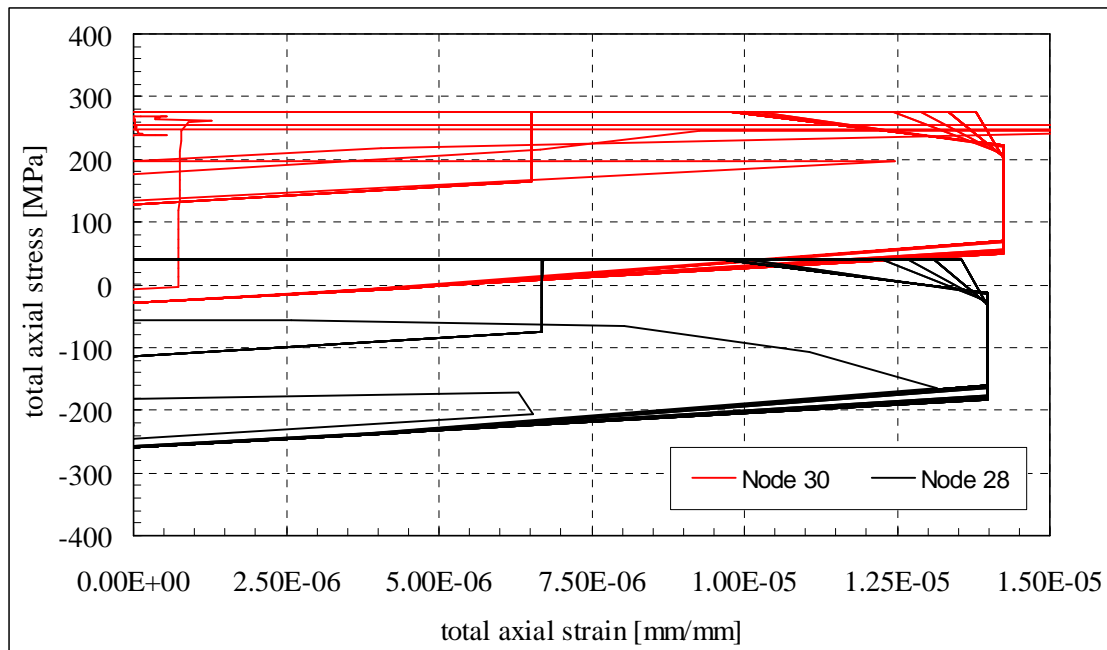


Figure 3.4-21b. Detail concerning the total transverse to weld stresses as a function of the corresponding strain for the inner (node 30) and outer (node 28) surface nodes of the safe-end/pipe joint WCL for Load history 5.

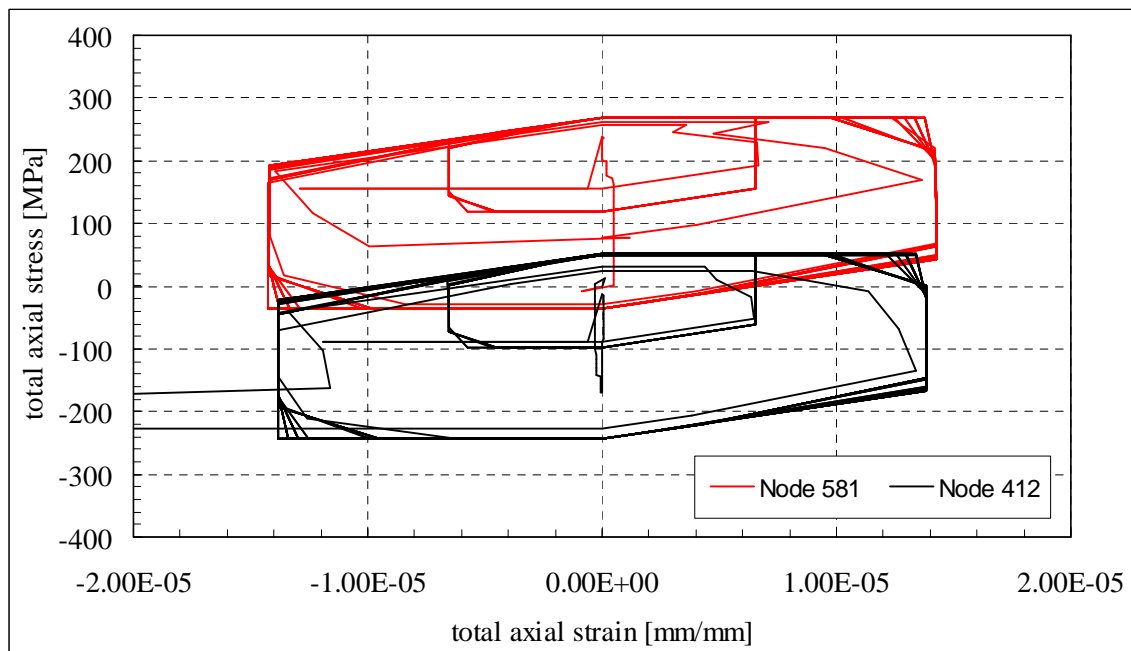


Figure 3.4-21c. The total transverse to weld stresses as a function of the corresponding strain for the inner (node 581) and outer (node 412) surface nodes of the safe-end/pipe joint WOL for Load history 5.

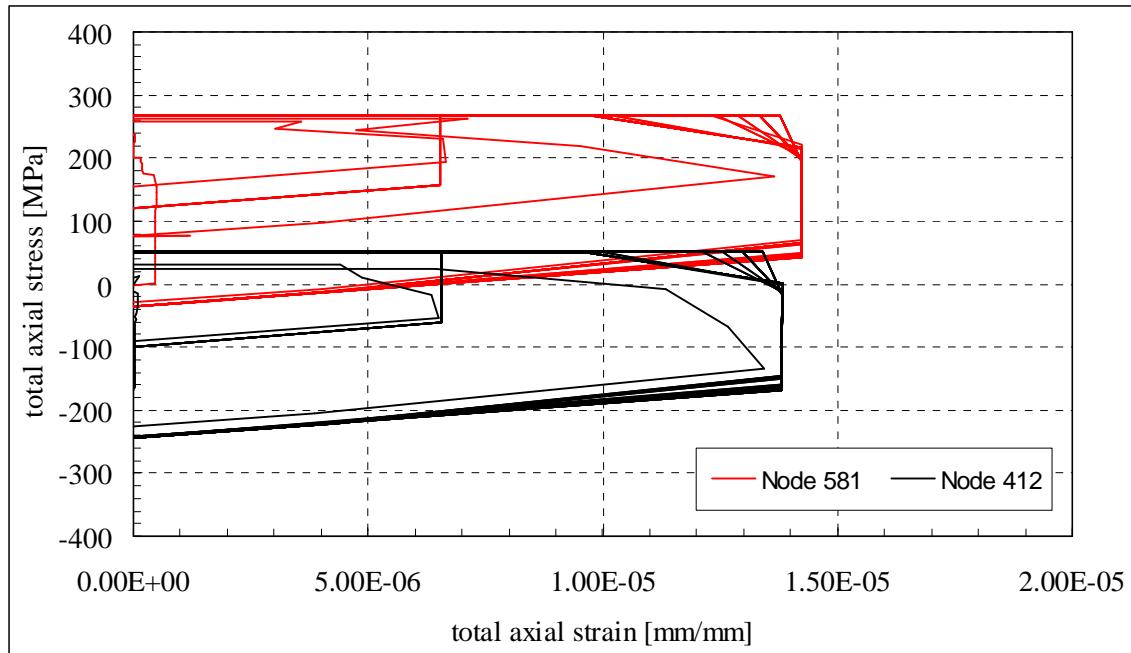


Figure 3.4-21d. Detail concerning the total transverse to weld stresses as a function of the corresponding strain for the inner (node 581) and outer (node 412) surface nodes of the safe-end/pipe joint WOL for Load history 5.

For the considered load histories the equivalent plastic strain results are presented for the safe-end/pipe joint weld centre line nodes 30 and 28 as a function of time as diagrams in Figures 3.4-22 and 3.4-23.

According to Abaqus documentation [13] the equivalent plastic strain, $\bar{\epsilon}_{eq}^P$, is defined as:

$$\bar{\epsilon}_{eq}^P = \bar{\epsilon}_{0,eq}^P + \int_0^t \dot{\bar{\epsilon}}^P dt \quad (3.4-1)$$

where $\bar{\epsilon}_{0,eq}^P$ is the initial equivalent plastic strain. The definition of $\dot{\bar{\epsilon}}^P$ depends on the material model. For von Mises plasticity this definition is:

$$\dot{\bar{\epsilon}}^P = \sqrt{\frac{2}{3} \cdot \dot{\epsilon}^P : \dot{\epsilon}^P} \quad (3.4-2)$$

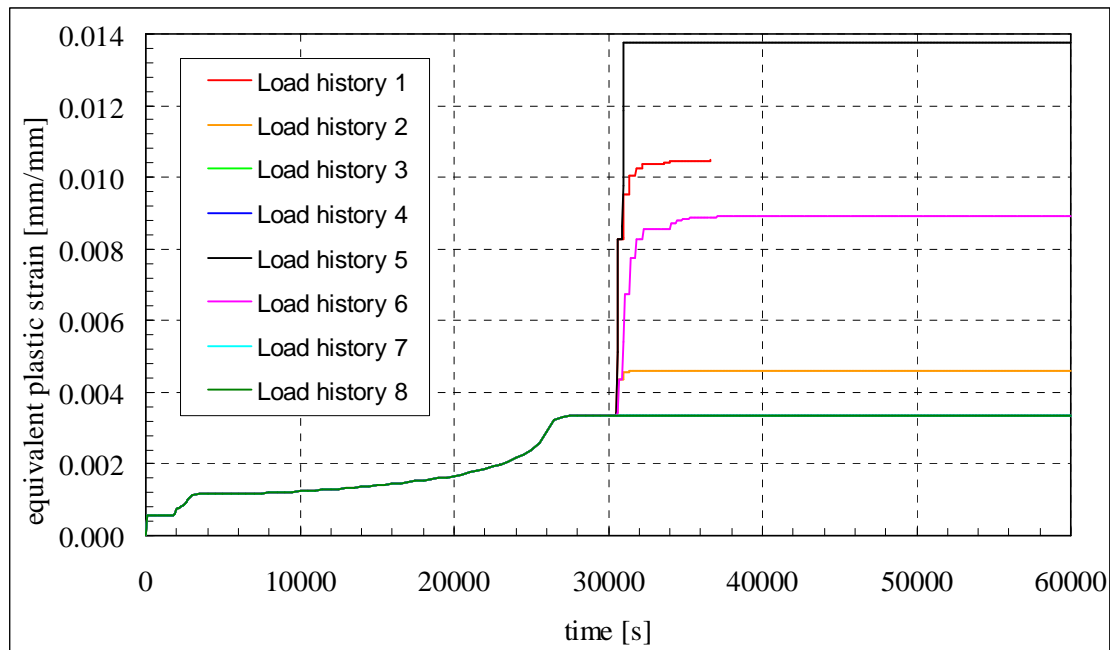


Figure 3.4-22. For the considered load histories the equivalent plastic strain results for WCL inner surface node 30 as a function of time.

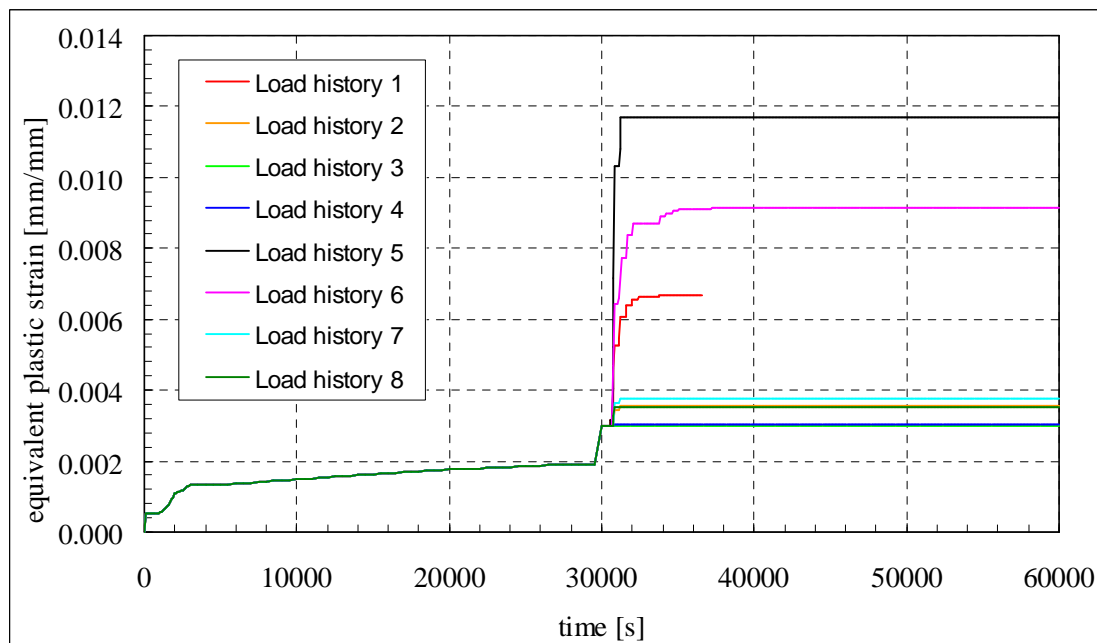


Figure 3.4-22. For the considered load histories the equivalent plastic strain results for WCL outer surface node 28 as a function of time.

As within the scope of the performed numerical simulations the changing of the WRSs ceased relatively soon, in all cases in less than ten load cycles, it did not seem meaningful enough to examine further the behaviour of the WRSs in this respect. Instead, it was investigated in more detail how the WRSs alter as a function of applied stress range and stress ratio.

Concerning the relaxation of the WRSs due to first load cycle as compared to that caused by the subsequent load cycles, it varied case specifically between approximately 50 and 80 % of the total WRS decrease. This is in line with what is described in many WRS relaxation assessment procedure source documents, see Section 4.2 in the other project report [10].

In the following is a brief description concerning the WRS simulation results in general:

- For Load histories 1 to 4, see Table 3.1.3-2, i.e. LCSs of Type 1; depending on the case, the WRSs ceased to change after 2 to 6 experienced LCs,
- For Load histories 5 to 8, see Table 3.1.3-2, i.e. LCSs of Type 2; depending on the case, the WRSs ceased to change after 2 to 5 experienced LCs,
- For all performed analyses the total stress exceeds the material yield strength in some regions of the component surfaces, e.g. in tension at WCL inner surface and in compression at WCL outer surface,
- In most cases and during at most the first five load cycles, the maximum strain values are approximately two times higher than those of corresponding saturated strain values,
- For all performed analyses, the load histories with larger stress load range decreased maximum WRS values more than those with smaller stress load range,
- For Load histories 1 to 4 in the weld centre line; the maximum WRS values in tension, which take place in node 30, decreased approximately from 28 to 60 %, depending on the case in question, whereas for maximum WRS values in compression, which take place in node 28, this decrease was negligible,
- For Load histories 5 to 8 in the weld centre line; the maximum WRS values in tension, which take place in node 30, decreased approximately from 22 to 48 %, depending on the case in question, whereas the maximum WRS values in compression, which take place in node 28, decreased approximately from 9 to 54 %, respectively,
- For all performed analyses in the weld centre line; within the wall the maximum WRS values both in tension and compression increased to some extent,
- For all performed analyses in the weld offset line; the maximum WRS values both in tension and compression decreased tens of percents both at inner & outer surface and slightly less so within wall.

4 Summary and suggestions for further research

According to experimental measurements and FEM analysis results the WRSs are typically relatively high in NPP component welds which are in as-welded state. Also, many NPP component welds have not been subject to any improvement treatment after manufacturing/installation, i.e. the welds remain in as-welded state. Thus it is of considerable importance to take the WRSs into account in the structural integrity analyses, e.g. crack growth sensitivity analyses. The residual stress distributions present in a structure are the result of the manufacturing history and the elastic-plastic properties of the structure. The former referring to the mechanical and thermal processes executed during the whole production sequence and the latter to the elastic-plastic behaviour of the structure.

The conditions/treatments that relieve residual stresses in NPP components include irradiation effects, thermal effects and mechanical load effects. In practise irradiation is not used to relax WRSs. Thus irradiation concerns mainly the RPV and its internals, as they are exposed to nuclear irradiation emanating from inside of the RPV, whereas its effect to other NPP systems and components is negligible. Thermal effects include annealing and PWHT, which are commonly used means to relieve the residual stresses. Also mechanical loads can relax the residual stresses, current techniques include e.g. shot-peening and vibratory stress relief.

Selection of suitable WRS distribution assumptions for structural integrity analyses is an issue requiring careful consideration. Several WRS assumption procedures are currently available, such as R6 Method, Rev. 4 [4], SINTAP procedure [5, 6], API 579 procedure [7] and FITNET procedure [8]. Here the SINTAP procedure was used, as the WRS assumptions it gives for welds connecting components of austenitic SS were the least over conservative within the considered scope of WRS assumption procedures. And unlike most of the other commonly used procedures, SINTAP also gave self-balancing WRS distribution in perpendicular to weld direction, which is realistic.

The wall thickness in the region of the examined safe-end/pipe joint weld is 16 mm. The initial WRS values for the examined weld were assumed according to the as-welded state WRS distribution equations of the SINTAP procedure [5, 6]. In this case they vary in perpendicular to weld direction linearly from 245 MPa in the inner surface to -245 MPa in the outer surface, for temperature of 286 °C.

The numerical simulations of the WRS distributions in this study were carried out with the same FEM model as was used in the previous part of the project, i.e. that consisting of a safe-end connecting to a nozzle and pipe, see ref. [3]. The scope of the analyses was extended so that here it was examined how the WRS distributions in the safe-end/pipe joint weld region behave under constant cyclic loading.

The performed analyses cover altogether eight loading histories, each being a constant amplitude load cycle sequence (LCS), and together spanning a representative range of loading conditions. This means that eight separate FEM analyses were carried out. The mentioned LCSs divide to two main types, with the axially oriented stress being the main cyclic load parameter. For the Type 1 the load range varies between 0 and 150 MPa, the stress ratio being in these cases 0. Whereas for the Type 2 the load range varies between -150 and 150 MPa, the stress ratio being in these cases -1, respectively. All prepared load histories include 50 load

cycles, which was a sufficient number to show how the WRSs change/decrease as a function of LCs in the simulations, if at all.

The ORNL material model, created by the Oak Ridge National Laboratory (ORNL) to describe the behaviour of austenitic SSs of types 304 and 316, see the Nuclear Standard NE F9-5T [14], was used in the performed FEM analyses for the weld, safe-end and pipe materials, respectively.

The scope of discussion concerning the ORNL material model is limited here to elastic-plastic analysis, i.e. the plasticity response, as within the operational temperature range of NPPs the effect of creep is negligible as compared to the plasticity response, and in general as well.

The issues described in this study concerning the ORNL material model are: initial and subsequent yield condition hardening rules, flow rule, bilinear representations of stress-strain curves, procedures for selecting or changing the size of the yield surface, selection of the maximum size of the yield surface, and thermoplastic effect.

Ziegler's hardening rule [15], generalized to the non-isothermal case, is used in Abaqus [13]. The Nuclear standard NE F9-5T [14] provides for some coupling between the plasticity and creep responses by allowing prior creep strain to expand and translate the subsequent yield surface in stress space. For SSs of types 304 and 316, however, prior plasticity does not change the subsequent creep response.

In the following is a brief description concerning the WRS simulation results:

- For all performed analyses the total stress exceeds the material yield strength in some regions of the component surfaces, e.g. in tension at weld centre line inner surface and in compression at weld centre line outer surface.
- For all performed analyses, the LCSs with larger stress load range decreased maximum WRS values more than those with smaller stress load range.
- For Type 1 load histories with stress ratio of 0; in the weld centre line the maximum WRS values in tension, which take place in inner surface, decreased approximately from 28 to 60 %, depending on the case in question, whereas for maximum WRS values in compression, which take place in outer surface, this decrease was negligible.
- For Type 2 load histories with stress ratio of -1; in the weld centre line the maximum WRS values in tension, which again take place in inner surface, decreased approximately from 22 to 48 %, depending on the case in question, whereas for maximum WRS values in compression, which again take place in outer surface, this decrease was approximately from 9 to 54 %, respectively.
- Concerning the relaxation of the WRSs due to first load cycle as compared to that caused by the subsequent load cycles, it varied case specifically between approximately 50 and 80 % of the total WRS decrease.
- For all performed analyses in the weld centre line; within the wall the maximum WRS values both in tension and compression increased to some extent.
- For all performed analyses in the offset line, which is located approximately 4.5 mm to the base material side from the weld edge; the maximum WRS values both in tension and compression decreased tens of percents both at inner & outer surface and slightly less so within wall.

The presented approach to assess numerically with FEM the relaxation of the WRSs could be well extended to other components having other materials and geometries without the needed computational work becoming too resource demanding.

Here an axisymmetric FEM model was used in the fully coupled thermal-stress/strain analyses. The next step could be to use a suitably optimised 3D FEM model in these analyses, or a coarser global 3D model in combination with a local but large enough and more densely meshed sub-model containing the region of interest, i.e. a weld. 3D modelling approach would also allow including bending loads.

One option to create local WRS distributions to a FEM model, that was due to work schedule limitations not attempted here, would be to use such values for the coefficient of thermal expansion in the weld region that the resulting stress field within the covered temperature range would match the desired WRS distribution. When using this approach the values of the coefficient of thermal expansion for the other material regions would be maintained in their original (i.e. correct) values or modified slightly.

Finally, the formation of the WRSs themselves could be examined via numerical simulations. Relevant guidance concerning this task will be provided e.g. in the next edition/revision of the R6 Method, see R5/R6 Newsletter [19]. Also this would necessitate the use of 3D FEM models, as manufacturing of circumferential (or any) weld is essentially a process taking place and causing effects three dimensionally.

5 Conclusions

Based on the conduct and outcome of the numerical FEM based simulations performed in this study it is concluded that this approach is feasible for modelling time dependently both the NPP components including the associated material properties, loads and boundary conditions, as well as the locally confined WRS fields and how they gradually alter/relax due to experienced repetitive mechanical load cycles.

One unfortunate departure from realism in case of some of the more recent WRS procedures, e.g. R6 Method Rev. 4, API 579 and FITNET, is that in the transverse to weld direction the WRSs are mostly not self-balancing. While making local crack growth calculations with a fracture mechanics based analysis tool this feature may not pose remarkable problems, but in case of corresponding 3D FEM analyses it is quite the other way around, as in order to achieve equilibrium FEM automatically modifies the WRSs towards self-balanced distributions over the component model walls, and thus the original WRS distributions are not maintained.

According to the above mentioned and other commonly used WRS assumption procedures, if a weld has not been in any improvement treatment, such as PWHT, the WRSs will not alter in service from the considerably high values corresponding to the as-welded state. When considering NPPs that have been in operation for decades, this assumption does not appear exactly realistic. Thus one motivation to numerically simulate the altering/relaxing of WRSs in NPP components that have experienced decades worth of typical transient load cases and operational conditions in general, stems from this background. With such assessment procedures the unnecessarily added conservatism in many computational structural integrity analyses could hopefully be to some extent decreased, which would consequently lead to more realistic analysis results.

For instance, the structural integrity analyses concerning stress corrosion cracking (SCC) typically include using crack growth equations having material and environment specific constant parameters the values for which have been defined as upper bound solutions based on the underlying laboratory measurement data. The ensuing crack growth sensitivity analysis results obtained using such equation parameter values, as unfortunately no best estimate alternatives are presently available, already show faster crack growth that in reality has been experienced in the plants. As the effect of SCC is time dependent, it remarkably increases the already conservative computed crack growth rates when including to considered loads also conservatively defined WRS distributions and even letting them remain in their maximum i.e. as-welded state values through crack growth sensitivity analyses spanning several decades of plant operation.

For all performed FEM simulations, in the weld centre line the maximum WRS values decreased both in tension and compression tens of percents both at inner and outer surface points, while the WRS values within the wall increased to some extent. For all performed FEM simulations, in the offset line which is located approximately 2.5 mm to the base material side from the weld edge, the maximum WRS values decreased both in tension and compression tens of percents both at inner and outer surface points and slightly less so within the wall.

References

1. Cronvall, O. Welding Residual Stress Relaxation in NPP Components Under Operation – A Literature Study. VTT Research report VTT-R-02200-10, Technical Research Centre of Finland (VTT), Espoo, Finland, 2010. 82 p.
2. Cronvall, O. Review and Comparison of Welding Residual Stress Definitions, VTT Research report VTT-R-01415-08. Espoo, Finland, 2008. 102 p.
3. Cronvall, O. Practical inclusion and behaviour of welding residual stresses in structural integrity analyses of NPP primary circuit components. VTT Research report VTT-R-00962-09, Technical Research Centre of Finland (VTT), Espoo, Finland, 2009. 53 p.
4. R6 Method; Assessment of the Integrity of Structures containing Defects, Revision 4. 2004 update of 2001 edition. British Energy (BE).
5. SINTAP; Structural Integrity Assessment Procedures for European Industry; Final Procedure: November 1999. Project funded by the European Union (EU) under the Brite-Euram Programme: Project No. BE95-1426, Contract No. BRPR-CT95-0024.
6. Barthelemy, J., Y., Janosch, J., J. Structural Integrity Assessment Procedures for European Industry; SINTAP; Task 4; Compendium of Residual Stress Profiles; Final Report: 18.5.1999. Project funded by the European Union (EU) under the Brite-Euram Programme: Project No. BE95-1426, Contract No. BRPR-CT95-0024. 40+18 pages.
7. American Petroleum Institute (API). Recommended practice for fitness-for-service. API 579. Washington, DC, American Petroleum Institute, 2000.
8. FITNET Fitness-for-Service PROCEDURE – FINAL DRAFT MK7. Editor(s) Koçak, M. et al. European Fitness-for-Service Thematic Network – FITNET. Germany. 1.5.2006.
9. Safety aspects of nuclear power plant ageing. Technical Report IAEA-TECDOC-540, International Atomic Energy Agency (IAEA), Vienna, Austria, January 1990. 200 p.
10. Cronvall, O. Welding Residual Stress Relaxation in NPP Components Under Operation – A Literature Study. VTT Research report VTT-R-02200-10, Technical Research Centre of Finland (VTT), Espoo, Finland, 2010.
11. ASME Boiler and Pressure Vessel Code, Section II. 2005 Update of 2004 Edition.
12. Abaqus/Standard User's manual, Version 6.8. Dassault Systèmes Simulia Corp., 2008. Providence, Rhode Island, U.S.A.
13. Abaqus Theory manual, Version 6.8. Dassault Systèmes Simulia Corp., 2008. Providence, Rhode Island, U.S.A.
14. Nuclear standard NE F9-5T, Guidelines and Procedures for Design of Class 1 Elevated Temperature Nuclear System Components. U.S. Department of Energy, Nuclear Energy Programs, September 1986, U.S.A.
15. Ziegler, H. A Modification of Prager's Hardening Rule. *Quart. Appl. Math.* 17 (1955) 55–65.
16. Sattari-Far, I., Andersson, M. Cladding Effects on Structural Integrity of Nuclear Components. SKI Report 2006:23, Statens kärnkraftinspektion (SKI), 2006. 73 p.
17. Crisfield, M. Non-Linear Finite Element Analysis of Solids and Structures, Volume 1: Essentials. John Wiley & Sons. Chichester, U.K., 1991. 345 p.

18. Brickstad, B. The Use of Risk Based Methods for Establishing ISI-Priorities for Piping Components at Oskarshamn 1 Nuclear Power Station. SAQ/FoU-Report 99/05, SAQ Kontroll AB, 1999. 83 p.
19. R5 and R6 Panels. R5/R6 Newsletter. Number 38, January 2009. 11 p.